THE INTERPLAY OF INTRINSIC DYNAMICS AND COUPLING IN SPATIALLY DISTRIBUTED NEURONAL NETWORKS

by

Jonathan D. Drover

M.S. Mathematics, University of Pittsburgh, 2000

B.A., College of Wooster, 1998

Submitted to the Graduate Faculty of

the School of Arts and Sciences in partial fulfillment

of the requirements for the degree of

Doctor of Philosophy

University of Pittsburgh

2005

UNIVERSITY OF PITTSBURGH

SCHOOL OF ARTS AND SCIENCES

This dissertation was presented

by

Jonathan D. Drover

It was defended on

June 14

and approved by

G. Bard Ermentrout, Department of Mathematics

Jonathan Rubin, Department of Mathematics

Stuart Hastings, Department of Mathematics

William Troy, Department of Mathematics

Nathan Urban, Department of Biological Sciences, CMU

Dissertation Director: G. Bard Ermentrout, Department of Mathematics

_____ G. Bard Ermentrout, Dissertation Director

THE INTERPLAY OF INTRINSIC DYNAMICS AND COUPLING IN SPATIALLY DISTRIBUTED NEURONAL NETWORKS

Jonathan D. Drover, PhD

University of Pittsburgh, 2005

We explore three coupled networks. Each is an example of a network whose spatially coupled behavior is drastically different than the behavior of the uncoupled system. 1. An evolution equation such that the intrinsic dynamics of the system are those near a degenerate Hopf bifurcation is explored. The coupled system is bistable and solutions such as waves and persistent localized activity are found. 2. A trapping mechanism that causes long interspike intervals in a network of Hodgkin Huxley neurons coupled with excitatory synaptic coupling is unveiled. This trapping mechanism is formed through the interaction of the time scales present intrinsically and the time scale of the synaptic decay. 3. We construct a model to create the spatial patterns reported by subjects in an experiment when their eyes were stimulated electrically. Phase locked oscillators are used to create boundaries representing phosphenes. Asymmetric coupling causes the lines to move, as in the experiment. Stable stationary solutions and waves are found in a reduced model of evolution/convolution type.

TABLE OF CONTENTS

LIST OF FIGURES

PREFACE

ACKNOWLEDGMENTS

I would like to thank the members of my committee, Prof. Jonathan Rubin, Prof. Stuart Hastings, Prof. W. Troy, and Prof. Nathan Urban. The insights and comments each made during the process of writing this thesis were extremely helpful.

Collaboration with Prof. Jonathan Rubin was an invaluable learning tool during my graduate career. The questions that he asked, as well as those that he answered, gave me new perspective and understanding of the problem at hand as well as the awareness of the basic questions that a researcher should ask when investigating a problem.

Prof. Stuart Hastings and Prof. W. Troy were each exceptional instructors. The courses that I took under each were stimulating and proved invaluable in producing this thesis. The comments made regarding this thesis aided in creating the strongest paper possible.

I thank Prof. Nathan Urban for serving on my committee. Working with University of Pittsburgh Students is not without precedent for Dr. Urban and I grateful that he could take the time to include me by sitting on my committee.

I am extremely grateful to my advisor, Prof. Bard Ermentrout, for an unparalleled research experience. My rise from computer illiteracy, the ability to read and write scientific papers, knowledge of the publication process, and the ability to speak to broad audiences are

all tangible results of working with Dr. Ermentrout. He provided undying support during my graduate career and allowed independence in my research.

1.0 INTRODUCTION

Dynamical systems can be used to describe most systems where variables evolve according to laws. Examples include biological, financial, chemical, and physical systems. In these systems, a particular variable, or quantification of a state can and usually will depend on the quantification of other elements of the network. This is represented by coupling in a dynamical system. On the other hand, it is often the case that the evolution of a variable depends on its current state. In this work we focus on the interplay between the *intrinsic* dynamics of a system, or the behavior of the system in the absence of coupling, and the mechanisms that couple individual oscillators together.

This dissertation consists of three parts. In each part we analyze a different network. In each of these networks the behavior of the uncoupled system is drastically different from the behavior of the network when coupling in introduced.

The first two problems presented here involve excitatory networks of neurons. These networks are capable of persistent activity and have been used to model phenomena such as wave propagation and short term memory [43, 12]. The types of solutions that we discuss for the first problem involve these explicitly. The second problem arose when a network of Hodgkin-Huxley neurons was shocked at an endpoint and the resulting solution rapidly synchronized.

The first problem concerns an evolution equation motivated by the Morris Lecar conductance based model. In the ML system, spiking behavior is separated from resting behavior by a branch of periodic solutions that originates at a subcritical Hopf bifurcation. The large amplitude stable solution forms when the branch of unstable periodic solutions folds around. The uncoupled system that we investigate is the normal form near a degenerate Hopf bifurcation. We consider the case where the rest state is stable so in the absence of coupling all solutions will collapse to rest. The terms that we use to couple the network are carefully selected so that they are of the correct order to remove the degeneracy. This induces both an excited state (stable periodic solution) and an unstable separatix (unstable periodic solution). In addition, the linear component of the coupling is arbitrarily small. This allows the rest state to remain locally stable regardless of the overall state of the network. The result is a parameter regime where there is bistability. Solutions connecting the two stable states, including waves and persistent regions of excitation, are demonstrated numerically and the mechanisms that are responsible for the different behaviors are discussed. Partial results of this work can be found in [18].

In the second part of this dissertation we discuss a subtle mechanism in the Hodgkin-Huxley conductance based model that causes long interspike intervals. A single oscillator is of type II excitability, as in the previous problem. We are concerned with the situation where the applied current to each individual cell is sufficient to sustain repeated spiking, so that each cell is inherently active (periodically spiking). We then couple the cells using excitatory synaptic coupling. The results of excitatory coupling in type II neurons are well known. First, the oscillators synchronize [30, 48] allowing one to approximate the behavior of the system using a single self coupled cell. Secondly, because the injected current is sufficient to

sustain oscillations we expect that the network will continue to fire. Numerical simulations of the model give unexpected results. The interspike interval (ISI) of the coupled network is unexpectedly long. In fact, the network spends more time in the silent phase (non-spiking) than it did in the absence of excitatory coupling.

The mechanism that causes the extremely lowered spiking frequency is a subtle trap that, when viewed from the appropriate frame of reference, resembles a fixed point of vortex type (complex conjugate pair of eigenvalues). The trap is formed by the interaction of the time scales of the uncoupled system and the time scale of the decay of a synaptic variable. The trap is represented as a curve of points in a phase plane when the synaptic variable is taken as a parameter. The linearization about this curve of points shows that this curve is indeed the working attractor and that it is the mechanism responsible for the delay. Comparisons between the approximations of release times about this curve of points and a curve defined by the intersection of nullclines [41, 42, 4] demonstrate the superiority of the trapping curve if one wants to analyze slow passage under certain conditions on the various time scales present in the problem. Results concerning the vortex can be found in [17].

The final problem in this thesis is motivated by an experiment performed by R.H.S. Carpenter [9]. A subject's eyes are exposed to alternating electrical current. When a light blocking object sweeps through the subject's field of vision, interrupting a uniformly lit field, parallel lines (phosphenes) are left in the wake of the retreating edge.

The model we use to recreate the patterns reported by the subjects is a rectangular grid of cells. Each uncoupled cells is of integrate and fire type, with a time dependent driving term. Parameters are chosen to lie in a regime such that each cell is phase locked 1:2 with the current. This yields a form of bistability, where each of the two phase locked solutions

act as attractors. The cells are connected using nearest neighbor coupling. The action of the coupling is to synchronize the network, pulling a node forward when it is behind its neighbors and holding a node back when it is ahead.

We construct a reduced model based on the full model. Like the full model, the intrinsic dynamics are bistable. Also, as in the full model, the coupling in the reduced model admits spatial uniformity as a locally stable solution.

For the full model and the reduced model the interplay between the intrinsic dynamics and the coupling architecture is a tug of war. The uncoupled network will settle into one of two behaviors. The coupling between two locations that are synchronized (or equal in the case of the reduced model) is zero. However, if neighboring nodes, or nearby points on the line for the reduced model, are assuming the opposite behavior the coupling may cause switching. This results in moving phase boundaries for the full model, and traveling wave solutions for the reduced model. If the coupling is sufficiently weak the phase boundaries in the full model will not move. In the reduced model, sufficiently small coupling results in the existence of stable stationary solutions with discontinuities. We prove the existence and linear stability of this type of solution.

2.0 A COUPLING INDUCED HOPF BIFURCATION

In this chapter we consider a continuous array of oscillators along the real line. The individual nodes (spatial locations) are excitable, meaning that an oscillator near threshold can become excited with a perturbation. We use excitatory coupling, so that a given location can exceed threshold when nearby oscillations can provide enough push.

Intrinsic oscillations typically occur via two mechanisms [36, 44]. In a type I neuron the oscillations occur because of a saddle node on a limit cycle bifurcation, where the threshold is a branch of a manifold extending from the saddle. A treatment of this type of coupled network using normal forms is given in [35]. The type of oscillators that we consider are type II. This means that the threshold is a branch of unstable periodic solutions that bifurcate from the rest state. We consider the case where this branch of periodic solution folds into a stable periodic solution. The configuration is shown in figure 2.0.1. For parameter values where a stable and unstable periodic solution coexist with a stable rest state there is bistability. The unstable periodic acts as a separatix and divides the plane into two basins of attraction.

Coupled systems near a subcritical Hopf bifurcation have been studied in [2, 33]. In these, the coupling analyzed is linear and so the coupling can determine the local stability properties of the resting state. The problem with this, from a neuronal standpoint, is that

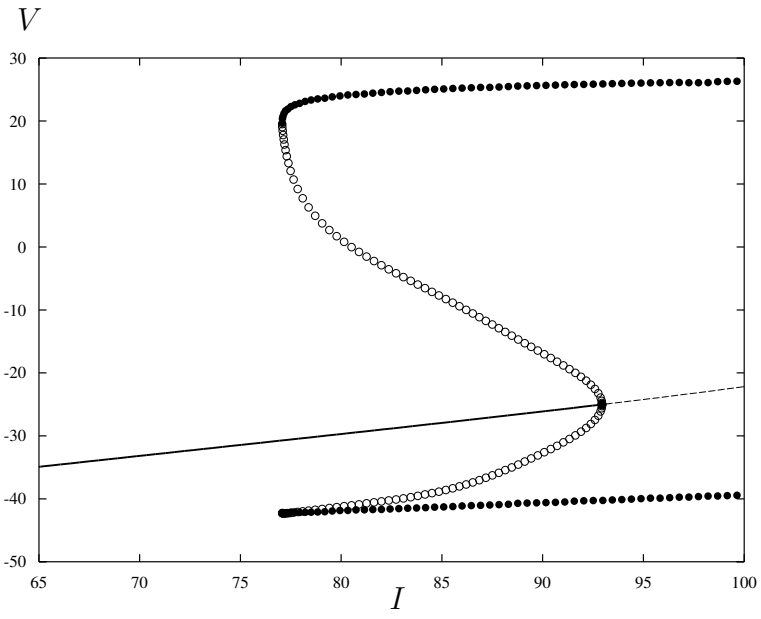

Figure 2.0.1: The described bistable regime. This is a bifurcation for the Morris Lecar neuronal model. The horizontal axis is the applied current and the vertical axis is the voltage. There is subcritical Hopf bifurcation for a value of I. This branch of periodic solutions turns around to form a stable periodic solution. Since the bifurcation is subcritical there is an interval of I such that the stable rest state coexists with the stable periodic orbit.

synaptic coupling is inherently nonlinear. The current state of a neuron, or coupled neurons, does not affect the stability of the rest state, at least when neighboring trajectories are in a neighborhood of the rest state. This can only happen if the coupling has nonlinear components, and linear components of the coupling are small relative to the linear components of the uncoupled system. This is unlike diffusive coupling (eg. gap junctions) where the presence of the coupling can change the resting state from attracting to repelling [22, 24, 40].

Our network is a normal form near a subcritical Hopf bifurcation. The uncoupled network has the form

$$z_t = z(\lambda + b|z|^2 + f|z|^4) \tag{2.1}$$

where b and f are complex and $\lambda = \lambda_1 + i\lambda_2$ is the bifurcation parameter. Equation (2.1) can be derived from any system near a Hopf bifurcation using a series of nonlinear changes of variables [53, 38].

The direction of bifurcating solutions depends on the real part of the coefficient b. If $Re(b) > 0$ then the bifurcation is subcritical and there is a branch of unstable periodic solutions in the direction of the stable rest state. If $Re(b) < 0$ the bifurcation is supercritical and the branch of periodics is stable, extending in the direction of the unstable equilibrium. If the real part of b vanishes, the bifurcation is degenerate. This is the Bautin Bifurcation. We assume in this chapter that $f = -1$. This term causes the branch of periodic solutions to fold into an outer branch. Dynamics near a Bautin bifurcation, particularly bursting, are explored in [37].

The system that we consider in this chapter is

$$z_t = z(\lambda + \imath q|z|^2 - |z|^4) + c\int_{-\infty}^{\infty} J(x-y)N(z)dy$$

where c is complex and $Re(c) > 0$. The function $N(z)$ is a polynomial in z such that $N(0) = 0$ and $N'(0) > 0$. In [2, 33] only terms linear in z are included. We will truncate $N(z)$ to include certain nonlinear terms. To motivate our choice of terms consider the following system consisting of two synaptically coupled neurons:

$$\begin{aligned}
\frac{dV_1}{dt} &= f(V_1) - gs_2(V_1 - V_{syn}) \\
\frac{ds_1}{dt} &= \alpha(V_1)(1-s_1) - \beta s_1 \\
\frac{dV_2}{dt} &= f(V_2) - gs_1(V_2 - V_{syn}) \\
\frac{ds_2}{dt} &= \alpha(V_2)(1-s_2) - \beta s_2
\end{aligned}$$

Assume that there is a rest state, V_{rest}, such that $f(V_{rest})$=0 and $\frac{\partial f}{\partial V}(V_{rest}) = -\eta < 0$ ensuring that the rest state is locally stable. In addition, suppose that $\alpha(V_{rest}) = 0$ and that $\alpha'(V_{rest}) = \epsilon > 0$. Under these condtions, $(V_i, s_i) = (V_{rest}, 0)$ is a fixed point for the coupled system. We assume that ϵ is sufficiently small so that the stability of the rest state for the uncoupled system is unaffected by the state of the rest of the network. To see this we consider the Jacobian matrix for the two cell system. Evaluated at the point $(V_{rest}, 0)$ with $\epsilon = 0$, this matrix is given by

$$\begin{pmatrix}
-\eta & 0 & 0 & -g(V_{rest} - V_{syn}) \\
0 & -\eta & -g(V_{rest} - V_{syn}) & 0 \\
0 & 0 & -\beta & 0 \\
0 & 0 & 0 & -\beta
\end{pmatrix}$$

The diagonal entries of this matrix are the eigenvalues, and each is negative. Because the real part of the eigenvalues will vary continuously with the entries of the matrix, there exists an $\epsilon > 0$ sufficiently small so that the eigenvalues remain in the left half of the complex plane.

Now, we extend the two cell system and consider M neurons coupled similarly to get the system

$$\frac{dV_i}{dt} = f(V_i) - g(v_i - V_{syn}) \sum_j w(i-j) s_j$$

$$\frac{ds_i}{dt} = \alpha(V_i)(1 - s_i) - \beta s_i$$

where the function $w(x) : \mathbb{R} \to [0, 1]$ is continuous, integrable and decreases as x gets farther from 0. In addition, we assume that $\sum_j w(j) = 1$.

Suppose that the time evolution of s is fast enough that for small changes in V near V_{rest} we can approximate s by solving

$$\alpha(V)(1 - s) - \beta s = 0$$

This gives a function $s = G(V)$ that we can expand around the point V_{rest}, thus obtaining a polynomial expression in V. We can use this expression to slave the coupling directly to the presynaptic potentials and get

$$\frac{dV_i}{dt} = f(V_i) - g(V_i - V_{syn}) \sum_j w_{i-j}[R(V_j - V_{rest}) + \epsilon(V_j - V_{rest})]$$

where R consists of the nonlinear terms in the expansion . In this paper we are concerned with the action of excitatory coupling and include only terms that contribute to excitement away from rest. This allows the simplification

$$\frac{dV_i}{dt} = f(V_i) - g(V_{rest} - V_{syn}) \sum_j w_{i-j}[R(V_j - V_{rest}) + \epsilon(V_j - V_{rest})]$$

Now, we consider the case $M = \infty$ and write the coupling as

$$\sum_{j=-\infty}^{\infty} w(i-j)G(V_j)$$

We assume that V is bounded. Since G is a polynomial in V it is bounded as well. Choose Δx and let $x_j = j\Delta x$. We write

$$\sum_{j=-\infty}^{\infty} w(x_i - x_j)G(V(x_j))\Delta x \tag{2.2}$$

We wish to take $\Delta x \to 0$. Since G is bounded and

$$\sum_{j=-\infty}^{\infty} w(j) = 1$$

we have that

$$\sum_{j=-\infty}^{\infty} w(j\Delta x) \leq \frac{1}{\Delta x} + w(0)$$

so that the following holds:

$$\sum_{j=-\infty}^{\infty} w(j\Delta x)G(V(j\Delta x)) \leq ||G||_\infty \sum_{j=-\infty}^{\infty} w(j\Delta x) \leq ||G||_\infty \left(\frac{1}{\Delta x} + w(0)\right)$$

Thus the sum (2.2) will converge as $\Delta x \to 0$ and we write the continuous model as

$$V_t(x,t) = f(V) - \hat{g}\int_{-\infty}^{\infty} J(x-y)[R(V(y,t) - V_{rest}) + \epsilon(V(y,t) - V_{rest})]dy$$

For this paper, the function R only contains the cubic terms that cannot be eliminated from the normal form using nonlinear changes of variables. All quadratic terms can be eliminated from the normal form near a Hopf bifurcation using nonlinear changes of variables (see [38, 53]). Because the cubic terms will dominate all higher order terms near rest, we omit higher order terms as well.

In this chapter, we discuss solutions to the equation

$$w_t = \lambda w + bw^2\bar{w} - w^3\bar{w}^2 + c\int_{-\infty}^{\infty} J(x-y)\left[w^2(y)\bar{w}(y) + \epsilon w(y)\right]dy \tag{2.3}$$

where $w(x,t) : (-\infty,\infty)\times(0,\infty) \to \mathbb{C}$. The parameters λ, b, c are complex and ϵ is small and real. The function J satisfies

$$J > 0$$

$$J < \infty$$

$$\int_{-\infty}^{\infty} J(x)dx = 1$$

$$J(-x) = J(x)$$

For all simulations in this section, assume that $J(x) = \frac{1}{2}e^{-|x|}$ unless otherwise stated.

Write $\lambda = \lambda_1 + i\lambda_2$ and (2.3) becomes

$$w_t = (\lambda_1 + \imath\lambda_2)w + bw^2\bar{w} - w^3\bar{w}^2 + cJ * (w^2\bar{w} + \epsilon w) \tag{2.4}$$

It is clear that when $\lambda_1 + c\epsilon = 0$ the linearized system has a pair of imaginary eigenvalues, indicating a Hopf bifurcation. The direction of the resulting periodic depends on the real part of the parameter $b + c$.

Make the substitution $w = z\exp(i\lambda_2 t)$ and (2.4) becomes

$$z_t = \lambda_1 z + bz^2\bar{z} - z^3\bar{z}^2 + cJ * (z^2\bar{z} + \epsilon z) \tag{2.5}$$

We are interested in parameter values that result in bistability. From this point on we assume that $\lambda_1 < 0$ so that the rest state $z = 0$ is stable. Also, we assume that the real component of all other parameters is non negative so that the Hopf bifurcation is subcritical. The other stable solution, a plane wave, will be shown to exist in section 2.2.1

We will analyze the near-Bautin network as follows

- We will analyze a two cell model to show which parameter regimes result in the behaviors we desire such as existence of stable solutions bounded away from zero coexisting with stable rest states.
- We show the linear stability of the bulk oscillations that occur when the entire network is excited. We prove that perturbations of the plane wave decay to zero with time when the wave number is small enough.
- We apply a theorem by X. Chen [10] to prove the existence and stability of waves for the case where $q = 0$.
- Numerically observe properties of the system for the $q \neq 0$ case where waves continue to exist. The important characteristics explored are the wave speed and phase gradient with respect to the 'twist' parameter, q. The waves are similar to those found in [23].
- Numerically observe properties of the system for the $q \neq 0$ case where there are no waves. We present a likely mechanism for bounded regions of persistent activity.

2.1 A TWO EQUATION MODEL

Consider the system of equations

$$\begin{aligned} z_1' &= \lambda z_1 + (b+iq) z_1^2 \bar{z} - z_1^3 \bar{z_1}^2 + (c_1 + ic_2)(z_2^2 \bar{z_2} + \epsilon z_2) \\ z_2' &= \lambda z_2 + (b+iq) z_2^2 \bar{z} - z_2^3 \bar{z_2}^2 + (c_1 + ic_2)(z_1^2 \bar{z_1} + \epsilon z_1) \end{aligned} \tag{2.6}$$

All parameters are real, and the imaginary component of the bifurcation parameter λ has been eliminated by the change of variables used to obtain equation (2.5). Note the coupling terms included in the two dimensional system. Consistent with the discussion in the introduction, these terms cannot be eliminated from the normal form. Other cubic terms that

cannot be similarly eliminated are discarded because they provide no contribution away from rest. That is, if

$$x_1' = f(x_1) + J * (x_1 g(x_1, x_2))$$

with $f(0) = 0$ and g quadratic the state $x_1 = 0$ is positively invariant. We only want terms that contribute to excitation away from rest, and therefore the only acceptable terms are those included in (2.6).

We begin by writing the equations in polar coordinates. Make the change of variables $z_j = r_j \exp(i\theta)$ to get the system

$$\begin{aligned} r_1' &= \lambda r_1 + b r_1^3 - r_1^5 + c_1 C(\theta)(r_2^3 + \epsilon r_2) + c_2 S(\theta)(r_2^3 + \epsilon r_2) \\ r_1 \theta_1' &= q r_1^3 + c_2 C(\theta)(r_2^3 + \epsilon r_2) - c_1 S(\theta)(r_2^3 + \epsilon r_2) \\ r_2' &= \lambda r_2 + b r_2^3 - r_2^5 + c_1 C(\theta)(r_1^3 + \epsilon r_1) - c_2 S(\theta)(r_1^3 + \epsilon r_1) \\ r_2 \theta_2' &= q r_2^3 + c_2 C(\theta)(r_1^3 + \epsilon r_1) + c_1 S(\theta)(r_1^3 + \epsilon r_1) \end{aligned} \tag{2.7}$$

where $C(\theta) = \cos(\theta_1 - \theta_2)$ and $S(\theta) = \sin(\theta_1 - \theta_2)$.

We want to explore the parameter regimes that allow a stable rest state to coexist with the stable large amplitude oscillation. Set $\phi = \theta_1 - \theta_2$ in (2.7) to get

$$\begin{aligned} r_1' &= \lambda r_1 + b r_1^3 - r_1^5 + c_1 (r_2^3 + \epsilon r_2) \cos(\phi) + c_2 (r_2^3 + \epsilon r_2) \sin(\phi) \\ r_2' &= \lambda r_2 + b r_2^3 - r_2^5 + c_1 (r_1^3 + \epsilon r_1) \cos(\phi) - c_2 (r_1^3 + \epsilon r_1) \sin(\phi) \\ \phi' &= q(r_1^2 - r_2^2) - c_1 \sin(\phi)(g(r_1, r_2) + g(r_2, r_1) + c_2 \cos(\phi)(g(r_2, r_1) - g(r_1, r_2)) \end{aligned} \tag{2.8}$$

where

$$g(x, y) = \frac{x^3 + \epsilon x}{y}$$

We seek the conditions on the parameters that lead to stable symmetric solutions, or solutions satisfying $r_1 = r_2$. In addition, we want the oscillators to be phase locked 1:1, so that $\phi' = 0$.

2.1.1 Symmetric Solutions

We seek solutions of the system (2.8) such that $R = r_1 = r_2$. If we assume solutions of this type, then (2.8)can be reduced to

$$\begin{aligned} R' &= \lambda R + bR^3 - R^5 + c_1(R^3 + \epsilon R)\cos(\phi) + c_2(R^3 + \epsilon R)\sin(\phi) \\ R' &= \lambda R + bR^3 - R^5 + c_1(R^3 + \epsilon R)\cos(\phi) - c_2(R^3 + \epsilon R)\sin(\phi) \\ \phi' &= -2c_1 \sin(\phi) g(R, R) \end{aligned} \tag{2.9}$$

It is obvious that the only possibilities are $\phi = 0$ or $\phi = \pi$. We consider the in phase solutions, or solutions of the form $R = r_1 = r_2$ and $\phi = 0$. This leaves us with the equation

$$R' = (\lambda + c_1\epsilon)R + (b + c_1)R^3 - R^5 \tag{2.10}$$

Solving for values of R where (2.10) vanishes we get the trivial solution $R = 0$ and the positive roots given by

$$R = \frac{1}{2}\sqrt{2(b + c_1) \pm \sqrt{(b + c_1)^2 + 4(\lambda + c_1\epsilon)}} \tag{2.11}$$

For ϵ sufficiently small the assumptions that $\lambda < 0$ and $b, c_1 \geq 0$ gaurantee the existence of two positive roots whenever $(b + c_1)^2 + 4(\lambda + c_1\epsilon) > 0$. This give us the existence condition

$$(b + c_1) > 2\sqrt{-\lambda - c_1\epsilon} \tag{2.12}$$

If we assume that

$$b + c_1 > 2\sqrt{-\lambda}$$

Then (2.12) will hold for $\epsilon > 0$.

This means that even when $b = 0$ we can still have a periodic solution for coupled system. If we set $b = 0$ then the condition is simply $c_1 > 2\sqrt{-\lambda - c_1\epsilon}$. The implications of this are

straightforward. If $b = 0$ then the Lyapunov coefficient in the normal form vanishes, and the Hopf bifurcation for the uncoupled system is degenerate. The direction of the bifurcating periodic solutions depends on the coupling. We assume that $b = 0$ for the remainder of the paper, as well as the condition

$$c_1 > 2\sqrt{-\lambda - c_1\epsilon}$$

so that the degeneracy is resolved and the existence of the periodic solutions is coupling induced.

We show that the symmetric phase locked solutions are stable. Linearizing the system (2.8) at the symmetric solutions yields

$$\begin{pmatrix} \alpha(R) & \beta(R) & \gamma(R) \\ \beta(R) & \alpha(R) & -\gamma(R) \\ a(R) & -a(R) & b(R) \end{pmatrix} \tag{2.13}$$

where $\alpha(R) = \lambda - 5R^4$, $\beta(R) = c_1(3R^2 + \epsilon)$, $\gamma(R) = c_2(R^3 + \epsilon R)$, $a(R) = 2qR - 4c_2R - 2\frac{c_2\epsilon}{R}$, and $b(R) = -2c_1(R^2 + \epsilon)$.

The characteristic polynomial for the matrix (2.13) is

$$(x - \alpha - \beta)(x^2 + (\beta - b - \alpha)x + \alpha b - \beta b - 2\gamma a)$$

This equation yields the following conditions for a symmetric in-phase solution to be stable:

$$\alpha + \beta < 0 \tag{2.14}$$

$$\beta - b - \alpha > 0 \tag{2.15}$$

$$\alpha b - \beta b - 2\gamma a > 0 \tag{2.16}$$

Along the lesser of the positive solutions we have that

$$R = \frac{1}{2}\sqrt{2(c_1) - 2\sqrt{(c_1)^2 + 4\lambda}}$$

Substituting this into (2.14) gives

$$\sqrt{c_1^2 + 4\lambda + 4c_1\epsilon}\left(c_1 - \sqrt{4\lambda + c_1^2 + 4\epsilon c_1}\right) + 2\epsilon c_1$$

Under the existence condition (2.12) this is real and positive. This implies that the inner branch of solutions is always unstable.

Similarly, substituting the outer solution into $\alpha + \beta$ gives the expression

$$\sqrt{c_1^2 + 4\lambda + 4c_1\epsilon}\left(-c_1 - \sqrt{c_1^2 + 4\lambda + 4\epsilon c_1}\right) + 2c_1\epsilon$$

For ϵ sufficiently small, this expression is negative, satisfying (2.14). It remains to check the other two conditions.

Substituting the outer solution into $\beta - b - \alpha$ we get the expression

$$5c_1^2 + 4\lambda + 10c_1\epsilon + 5c_1\sqrt{c_1^2 + 4(\lambda + c_1\epsilon)}$$

Because $c_1^2 + 4(\lambda + \epsilon c_1) > 0$ the condition (2.15) is satisfied.

Rewrite the condition (2.16) as

$$F(c_2) = Ac_2^2 + Bc_2 + C > 0$$

where

$$A = 8\lambda + 4c_1^2 + 12c_1\epsilon + 4(c_1 + \epsilon)\sqrt{c_1^2 + 4\lambda + 4c_1\epsilon}$$

$$B = -q(2(\epsilon + c_1)\sqrt{c1^2 + 4\lambda + 4c_1\epsilon} + 4\lambda + 2c_1^2 + 6\epsilon c_1) = -qD$$

$$C = 4c_1\left[(\lambda + 4c_1\epsilon + 2c_1^2)\sqrt{c_1^2 + 4\lambda + 4c_1\epsilon} + 4c_1(5\lambda + 2c_1^2) + 8\epsilon(\lambda + 4c_1^2 + 2c_1\epsilon)\right]$$

A, D, and C are all positive under the assumed conditions on the parameters. Thus, if $c_2 = 0$ then we have that $C > 0$ and condition (2.16) is satisfied. Suppose that $c_2 > 0$. Because $D > 0$, there can always be a q sufficiently large so that $F(c_2) < 0$. At the critical value of $q = q^*$, a single eigenvalue crosses the $x = 0$ axis. This destabilizes the equilibrium.

For the remainder of this chapter we assume that $c_2 = 0$ so that the stable periodic is stable for any q. We will also assume that

$$c_1 > 2\sqrt{-\lambda - \epsilon c_1}$$

$$\lambda + \epsilon c_1 < 0$$

so that the outer branch of symmetric oscillations exists and the network lies in a bistable parameter regime.

2.2 THE INTEGRO-DIFFERENTIAL EQUATION

Consider a generalization of the two equation system

$$z_{i_t} = z_i(\lambda + \imath q|z_i|^2 - |z_i|^4) + c \sum_{j=-\infty, j\neq i}^{\infty} \omega_{i,j}(z_j^2\overline{z_j} + \epsilon z_j) \tag{2.17}$$

where all parameters are the same as before. The interaction weights $\omega_{i,j} = \omega(i-j)$ are non-negative and decrease as $i - j$ gets further from zero. We normalize so that

$$\sum_{j=-\infty, j\neq i}^{\infty} \omega_{i,j} = 1$$

for every i. An important difference between the system (2.17) and the two equation system is that the oscillators need not be synchronized for there to be a symmetric solution ($|z_i| =$

$R^2 \forall i$)away from zero. Again, make the change of variables $z_i = r_i e^{\imath\theta_i}$ to get the evolution equation for θ

$$r_i\theta_i' = qr_i^3 + c\sum_{j\neq i}\omega_{i,j}\sin(\theta_j - \theta_i)(r_j^3 + \epsilon r_j) \tag{2.18}$$

At this point we define the phase gradient of a solution to be the first spatial derivative of θ. For the discrete case it is the difference between the θ values in consecutive nodes. If we assume that $r_i = R$ for every i, then any constant phase gradient is time invariant, and in turn uniform amplitude is time invariant. This is different from the two equation system since the oscillators had to be synchronous in order for the symmetry to persist. Now consider the evolution equation for the amplitude component of z_i

$$r_i' = r_i(\lambda - r_i^4) + c\sum_{j}\omega_{i,j}\cos(\theta_j - \theta_i)(r_j^3 + \epsilon r_j) \tag{2.19}$$

If we assume once more that $r_i = R$ for all i, and assume a constant phase gradient we may rewrite as

$$R' = R(\lambda + \epsilon c\eta - R^4) + c\eta R^3$$

where

$$\eta = \sum_{j}\omega(i-j)\cos(\theta_j - \theta_i)$$

The right side is independent of i, seen by making the change of variables $l = i - j$

$$\eta = \sum_{l}\omega(l)\cos(kl)$$

where k is the phase gradient. This is similar to equation (2.10) with $b = 0$. Correspondingly, we expect that the outer branch of periodic solutions will exist and if the condition

$$c\eta > 2\sqrt{-\lambda - \epsilon c\eta}$$

holds. For large phase gradients result in small values of η we expect that if the oscillations are sufficiently desynchronized the plane wave solution can cease to exist.

The continuous analog to equation (2.17) is

$$z_t = \lambda z + iqz^2\bar{z} - z^3\bar{z}^2 + (c_1 + ic_2)\int_{-\infty}^{\infty} J(x-y)\left[z^2(y)\bar{z}(y) + \epsilon z(y)\right] dy \tag{2.20}$$

where $z \in \mathbb{C}$ and all parameters are the same as for the two dimensional system. As for the two equation model, we let $c_2 = 0$, so that the synchronous solution $z = \rho\exp(i\Omega t)$ is always stable, for some Ω.

We now show, for the existing conditions imposed on the parameters, the linear stability of the plane wave solution to (2.20).

2.2.1 Plane Wave Solutions

Consider solutions of (2.5) of the form

$$z(x,t) = \rho\exp(i(\Omega t - kx)) \tag{2.21}$$

Substituting (2.21) into (2.5) gives

$$i\rho\Omega\exp(i(\Omega t - kx)) = \rho\exp(i(\Omega t - kx))(\lambda + iq\rho^2 - \rho^4)$$

$$+c_1\int_{-\infty}^{\infty} J(x-y)(\rho^3 + \epsilon\rho)\exp(i(\Omega t - ky))dy$$

Simplification results in

$$i\Omega = \lambda + iq\rho^2 - \rho^4 + (\rho^2 + \epsilon)c_1\int_{-\infty}^{\infty} J(x-y)\exp(ik(x-y))dy$$

Letting $\hat{J}(k) = \int_{-\infty}^{\infty} J(s)\exp(iks)ds$ gives

$$i\Omega = \lambda + iq\rho^2 - \rho^4 + c_1(\rho^2 + \epsilon)\hat{J}(k)$$

Separating real and imaginary parts yields

$$\Omega = q\rho^2 + c_1(\rho^2 + \epsilon)Im(\hat{J}(k))$$

with ρ determined by

$$\lambda - \rho^4 + c_1(\rho^2 + \epsilon)Re(\hat{J}(k)) = 0$$

Because J is symmetric $Im(\hat{J}(k)) = 0$ and so the equations become

$$\Omega = q\rho^2$$

$$\lambda - \rho^4 + c_1(\rho^2 + \epsilon)\hat{J}(k) = 0$$

The existence of the plane waves is shown. We now show that the plane waves of sufficiently small wave number are linearly stable.

Let

$$z(x,t) = \rho\exp(i(\Omega t - kx)) + w(x,t) \tag{2.22}$$

where $w(x,t) : \mathbb{R} \times [0,\infty) \to \mathbb{C}$ is a small perturbation. Substitute (2.22) into (2.5) and take terms linear in w to obtain the expression

$$w_t = f(w) + c_1 \int_{-\infty}^{\infty} J(x-y)(\rho^2 e^{2i(\Omega t - ky)}\bar{w} + (2\rho^2 + \epsilon)w)dy \tag{2.23}$$

where

$$f(w) = \lambda w + iq\rho^2(2w + e^{2i(\Omega t - kx)}\bar{w}) - \rho^4(3w + 2e^{2i(\Omega t - kx)}\bar{w})$$

We wish to show that $w \to 0$ as $t \to \infty$. Let $w = \exp(i(\Omega t - kx))v$ and substitute into (2.23) to get the equation

$$\begin{aligned} \imath\Omega v + v_t = \quad & \lambda v + \imath q\rho^2(2v + \bar{v}) - \rho^4(3v + 2\bar{v}) \\ & + c\int_{\mathbb{R}} J(x-y)\left[\rho^2 e^{\imath k(x-y)}\bar{v} + (2\rho^2 + \epsilon)e^{\imath k(x-y)}v\right] dy \end{aligned} \tag{2.24}$$

The coupling can be written as

$$c\int_{\mathbb{R}} J(s)e^{\imath k(s)}\left[\rho^2\bar{v}(x-s) + (2\rho^2+\epsilon)v(x-s)\right] ds \tag{2.25}$$

Separating the real and imaginary parts of (2.25) gives

$$c\int_{\mathbb{R}} J(s)\left[(3\rho^2+\epsilon)\cos(ks)v_1(x-s) - (\rho^2+\epsilon)\sin(ks)v_2(x-s)\right] ds \tag{2.26}$$

$$c\int_{\mathbb{R}} J(s)\left[(\rho^2+\epsilon)\cos(ks)v_2(x-s) + (3\rho^2+\epsilon)\sin(ks)v_1(x-s)\right] ds \tag{2.27}$$

where $v = v_1 + \imath v_2$. Equation (2.26) is the real component of the coupling, and (2.27) is the imaginary component. Separating the uncoupled system into real and imaginary components and combining with equations (2.26)- (2.27) yields the following system

$$-\Omega v_2 + v_{1t} = \lambda v_1 - q\rho^2 v_2 - 5\rho^4 v_1 + A_1(v_1, v_2, x) \tag{2.28}$$

$$\Omega v_1 + v_{2t} = \lambda v_2 + 3q\rho^2 v_1 - \rho^4 v_2 + A_2(v_1, v_2, x) \tag{2.29}$$

where $v = v_1 + \imath v_2$ and $A_i(v_1, v_2, x)$ denote the expressions (2.26) and (2.27), respectively. Since we have that $\Omega = q\rho^2$ on the plane wave equations (2.28)- (2.29) simplify to

$$v_{1t} = \lambda v_1 - 5\rho^4 v_1 + A_1(x) \tag{2.30}$$

$$v_{2t} = \lambda v_2 + 2q\rho^2 v_1 - \rho^4 v_2 + A_2(x) \tag{2.31}$$

We define the linear operator L to be

$$L\vec{v} = -\frac{\partial}{\partial t}\vec{v} + \begin{pmatrix} \lambda - 5\rho^4 + c(3\rho^2+\epsilon)J_c * (\cdot) & c(\rho^2+\epsilon)J_s * (\cdot) \\ 2q\rho^2 - c(3\rho^2+\epsilon)J_s * (\cdot) & \lambda - \rho^4 + c(\rho^2+\epsilon)J_c * (\cdot) \end{pmatrix} \vec{v}$$

where $\vec{v} = (v_1, v_2)$, $J_c = J(x)\cos(kx)$, and $J_s = J(x)\sin(kx)$. We look for bounded solutions satisfying $L\vec{v} = 0$. We consider solutions of the form $v_1 = e^{\alpha t}e^{ilx}u_1$ and $v_2 = e^{\alpha t}e^{ilx}u_2$ where u_1 and u_2 are constants. We aim to show that for certain values of k these eigenfunctions will decay to zero, corresponding to a stable manifold connected to the plane wave solution. Since J is assumed to be even, the coupling expression (2.26) becomes

$$\begin{aligned} ce^{\alpha t}e^{ilx} \quad & \int_{\mathbb{R}} J(s)\left[(3\rho^2+\epsilon)\cos(ks)\cos(ls)u_1\right] ds \\ & +\imath c e^{\alpha t}e^{ilx}\int_{\mathbb{R}} J(s)\left[(\rho^2+\epsilon)\sin(ks)\sin(ls)u_2\right] ds \end{aligned} \tag{2.32}$$

and, similarly, the expression (2.27) can be written

$$\begin{aligned} ce^{\alpha t}e^{ilx} \quad & \int_{\mathbb{R}} J(s)\left[(\rho^2+\epsilon)\cos(ks)\cos(ls)u_2\right] ds \\ & -\imath c e^{\alpha t}e^{ilx}\int_{\mathbb{R}} J(s)\left[(3\rho^2+\epsilon)\sin(ks)\sin(ls)u_1\right] ds \end{aligned} \tag{2.33}$$

The system $L\vec{v} = 0$ can be written as

$$\alpha \begin{pmatrix} u_1 \\ u_2 \end{pmatrix} = \begin{pmatrix} \lambda - 5\rho^4 + c(3\rho^2+\epsilon)J_{cc} & +\imath c(\rho^2+\epsilon)J_{ss} \\ 2q\rho^2 - \imath c(3\rho^2+\epsilon)J_{ss} & \lambda - \rho^4 + c(\rho^2+\epsilon)J_{cc} \end{pmatrix} \begin{pmatrix} u_1 \\ u_2 \end{pmatrix} \tag{2.34}$$

where

$$J_{ss} = \int_{-\infty}^{\infty} J(s)\sin(ks)\sin(ls)ds$$

and

$$J_{cc} = \int_{-\infty}^{\infty} J(s)\cos(ks)\cos(ls)ds$$

These function can be expressed in terms of the Fourier Transform, $\hat{J}(k)$, of the interaction function

$$J_{cc} = \frac{1}{2}\hat{J}(k+l) + \frac{1}{2}\hat{J}(k-l)$$

$$J_{ss} = -\frac{1}{2}\hat{J}(k+l) + \frac{1}{2}\hat{J}(k-l)$$

The top panel of figure 2.2.1 shows that , for $k = 0$, the real part of the greatest eigenvalue is negative for all $l \neq 0$. The middle panel shows that for $k = 0.5$ small perturbations from the plane wave will grow since the real part of the eigenvalue is positive. The lower left panel shows that for a $k > 0$ there is a stable corresponding plane wave. Thus there must be an interval surrounding $k = 0$ such that the perturbation goes to zero, and hence the plane wave is stable (linearly). This result extends to the case of any J such that $\hat{J}(k)$ decreases as k gets farther from 0.

Under the conditions imposed on the parameters, we have shown that there is both a stable rest state at $z = 0$ and a stable plane wave of the form (2.21).

2.2.2 Traveling Wavefronts (The $q = 0$ case)

In this section we show that under the conditions set previously on the parameters there are traveling wave solutions connecting the stable rest state to the stable plane wave solution for the case $q = 0$. That is, there is a solution to (2.5) such that

$$z(x,t) = h(x - ct)\rho e^{i(\Omega(k)t - kx)} \tag{2.35}$$

where $h(-\infty) = 1$ and $h(\infty) = 0$.

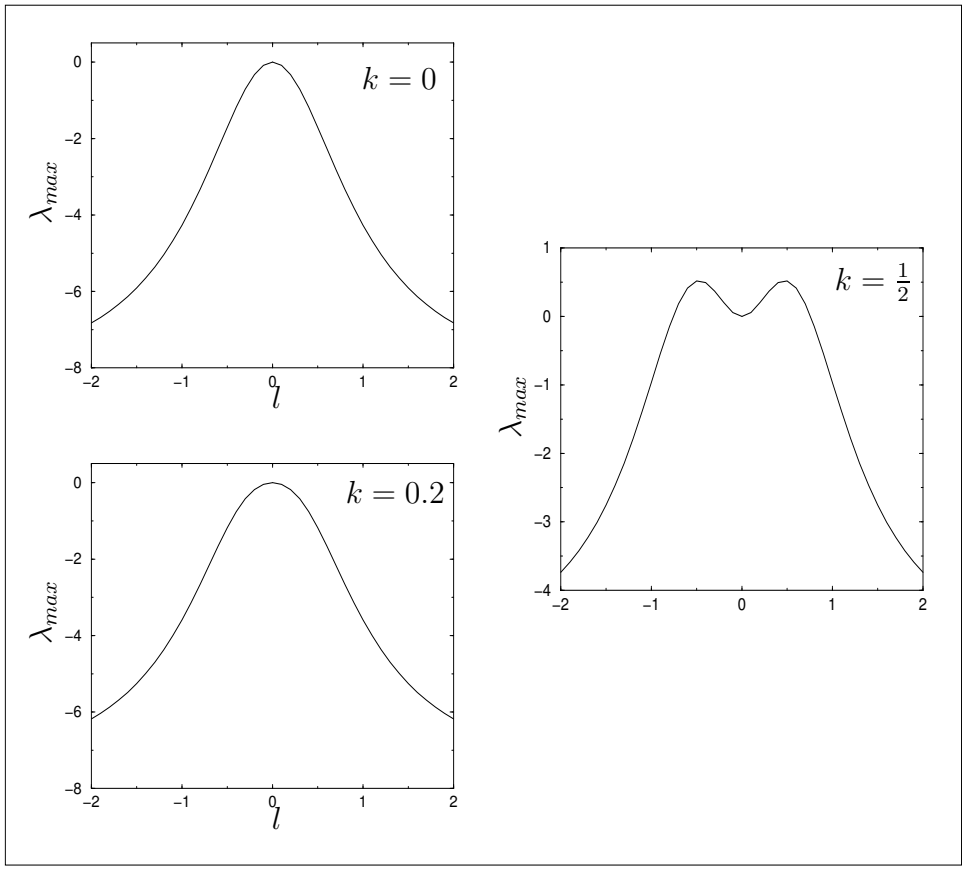

Figure 2.2.1: Stability of the plane wave. The left panels show values of k, the wave number, such that the greatest eigenvalue of the system (2.34) (vertical axis) is negative, corresponding to a linearly stable plane wave. The right panel shows that for sufficiently large k the plane wave destabilizes. In all panels, the horizontal axis is l, the rotation of the eigenfunction $u_i e^{ilx}$ that corresponds to a stable manifold.

We begin by making the change of variables $z = re^{i\theta}$. Then (2.5) becomes:

$$r_t = \lambda r - r^5 + c_1 \int_{-\infty}^{\infty} J(x-y)(r^3(y) + \epsilon r(y)) \cos(\theta(y) - \theta(x)) dy \tag{2.36}$$

$$r\theta_t = qr^3 + c_1 \int_{-\infty}^{\infty} J(x-y)(r^3(y) + \epsilon r(y)) \sin(\theta(y) - \theta(x)) dy \tag{2.37}$$

If we assume that $q = 0$, then (2.37) becomes

$$r\theta_t = c_1 \int_{-\infty}^{\infty} J(x-y)(r^3(y) + \epsilon r(y)) \sin(\theta(y) - \theta(x)) dy \tag{2.38}$$

Note that $\theta(x) = C$ is a solution to (2.38). That is, having a zero phase gradient is time invariant. Under the assumption that $\theta(x) = C$, the system defined by (2.36) and (2.38) is reduced to

$$\rho' = \lambda\rho - \rho^5 + c_1 \int_{-\infty}^{\infty} J(x-y)(\rho^3(y) + \epsilon\rho(y)) dy \tag{2.39}$$

We show that there exists a unique (up to a translation), asymptotically stable traveling front that satisfies (2.35) ($k = 0$) and is a solution to (2.39) by application of the following theorem:

Theorem 1 *Chen, [10]*

Consider the evolution equation

$$u_t = Du_{xx} + G(u, J_1 * S^1(u), ..., J_n * S^n(u)) \tag{2.40}$$

where $J * S(u)$ stands for the convolution $\int_R J(x-y)S(u(y))dy$. Assume:

1. *For some $a \in (0,1)$, the function $f(u) = G(u, u, ..., u)$ satisfies $f > 0$ in $(-1, 0) \cup (a, 1)$, $f < 0$ in $(0, a) \cup (1, 2)$, and $f'(0) < 0$, $f'(a) > 0$, and $f'(1) < 0$.*

2. *For each* $i = 1, ..., n$, *the kernel* J_i *is* C^1 *and satisfies* $J_i(.) \geq 0$, $\int_R J_i(y)dy = 1$, *and* $\int_R J_i(y)dy < \infty$.

3. *The functions* $G(u,p)$ $(p = (p_1, ..., p_n))$, *and* $S^1(u), ..., S^n(u)$ *are smooth functions satisfying* $\forall u \in [-1,2]$, $p \in [-1,2]^n$, $i = 1, ..., n$, $G_{p_i}(u,p) \geq 0$, $S^i_u(u) \geq 0$.

4. *Either* $D > 0$ *or* $G_u(u,p) < 0$ *and* $G_{p_1}(u,p)S^1_u(u) > 0$ *on* $[-1,2]^{n+1}$.

If conditions 1-4 hold, there exists a unique (up to a translation) asymptotically stable monotone traveling wave connecting 0 *to* 1.

For our system

$$G(u, J^1 * S^1, J^2 * S_2) = \lambda u - u^5 + c_1 J * \epsilon u + c_1 J * u^3$$

$$G(u,u,u) = (\lambda + \epsilon c_1)u - u^5 + c_1 u^3$$

$$G_u(u,p) = \lambda - 5\rho^4$$

$$S^1(u) = \epsilon u$$

$$s^2(u) = u^3$$

$$G_{p_i}(u,p) = c_1$$

$$S^1_u(u) = \epsilon$$

$$S^2_u(u) = 3u^2$$

The first condition in the theorem requires that the system be bistable. As has been the case throughout this paper, we are assuming that $c_1 > 2\sqrt{-\lambda}$. It has been shown previously that if this condition holds then there are two stable solutions separated by an unstable separatix.

The second condition is satisfied under the conditions that we have set on the interaction function J.

The third condition requires that $G_p = c_1 \geq 0$ and $S_u^i(u) \geq 0$. Both of these are satisfied.

The fourth condition is also satisfied, since $\lambda - 5u^4 < 0$ for any u. We have that $G_{p_1}(u,p) = c_1 > 0$ and $S_u^1(u) = \epsilon > 0$.

We may conclude that there exists a traveling wave connecting the stable rest state at $u = 0$ to the non rotating plane wave (fixed point). This only applies to the $q = 0$ case. We expect that the wave will continue to exist for values of q in a neighborhood of $q = 0$, but have no formal proof. Numerical simulations suggest that these waves exist, and we discuss these waves in the next subsection.

It is interesting to note that the wave is shown to exist for every $\epsilon > 0$ allowed by the work in previous sections. However, the theorem does not apply to the case $\epsilon = 0$. The difficulty is that one cannot, using the machinery in Chen's proof, show that the following comparison lemma holds:

Lemma 1 *Chen's Lemma*

There exists a positive continuous function $\eta(x,t)$ defined on $[0,\infty) \times (0,\infty)$ such that if $u(x,t)$ and $v(x,t)$ satisfy $-1 \leq u, v \leq 2$,

$$u_t \geq G(u, J * S^1(u), J * s^2(u))$$

$$v_t \leq G(v, J * S^1(v), J * S^2(v))$$

and $u(\cdot,0) \geq v(\cdot,0)$, then

$$u(x,t) - v(x,t) \geq \eta(|x|,t) \int_0^1 [u(y,0) - v(y,0)]dy$$

for all $x \in R$, $t > 0$.

To proof this Chen uses a positive lower bound on the function

$$\hat{J}(x,y,t) = \int_0^1 \sum_{i=1}^{2} G_{p_i}(w, J * S^1(w), J * S^2(w))(x,t) S_u^i(w)(y,t)|_{w=u+\theta v} d\theta$$

This bound needs to be independent of initial conditions. If $\epsilon = 0$ then $S_u^i(0) = 0$. Thus, initial conditions can be chosen to make this arbitrarily small, and no uniform lower bound is possible. It is not apparent whether or not the comparison in Chen's Lemma holds.

The problem as $\epsilon \to 0$ is that the wave could 'flatten out'. Let $U_\epsilon(x - ct) = u_\epsilon(x,t)$ be the traveling wave solution to (2.39). Shift it so that $U_\epsilon(0) = A$, where A is the unstable separatix. For any $0 < \epsilon \ll 1$ we know that $U_\epsilon'(0) < 0$. One needs to show that

$$\lim_{\epsilon \to 0} U_\epsilon'(0) = \beta < 0$$

We can resolve the existence of the wave for $\epsilon = 0$ by converting the integral equation to a system of differential equations. For this we assume that

$$J(x) = \frac{1}{2} e^{-|x|}$$

The Fourier transform of this function is

$$\hat{J}(k) = \frac{1}{1 + k^2}$$

Let

$$A(x,t) = \int_{\mathbb{R}} J(x - y) R(y)^3 dy$$

Using a Fourier transform we get that

$$A - A_{xx} = R^3$$

Now, since we are looking for traveling waves with constant velocity, let $\zeta = x - \eta t$ to get

$$-\eta R'(\zeta) = \lambda R(\zeta) - R(\zeta)^5 + cA(\zeta)$$

$$A''(\zeta) = A(\zeta) - R(\zeta)^3$$

Let $A_1 = A'$ to get a 3-dimensional system of first order ODEs

$$R' = -\tfrac{1}{\eta}\left(\lambda R - R^5 + cA\right)$$

$$A' = A_1$$

$$A_1' = A - R^3$$

This system has three fixed points (u^*, A^*, A_1^*) at

$$(0,0,0)$$

$$\left(\sqrt{\frac{c+\sqrt{c^2+4\lambda}}{2}}, \left(\sqrt{\frac{c+\sqrt{c^2+4\lambda}}{2}})\right)^3, 0\right)$$

$$\left(\sqrt{\frac{c-\sqrt{c^2+4\lambda}}{2}}, \left(\sqrt{\frac{c-\sqrt{c^2+4\lambda}}{2}}\right)^3, 0\right)$$

Numerical simulations of the system of ODEs suggest that for η small the unstable manifold extending from the origin passes through the R axis to the left of the fixed point with the largest R component. For large η this manifold crosses the vertical line

$$R = \sqrt{\frac{c+\sqrt{c^2+4\lambda}}{2}}$$

in the $R - A_1$ plane below the R axis. This suggests that there is a shooting argument to prove the existence of a heteroclinic solution connecting the fixed points. We performed the shooting argument numerically to find a heteroclinic connecting the outer fixed points. This orbit is shown in the $R - A_1$ plane in figure 2.2.2. The solutions shown exists for $\eta = 3.884$.

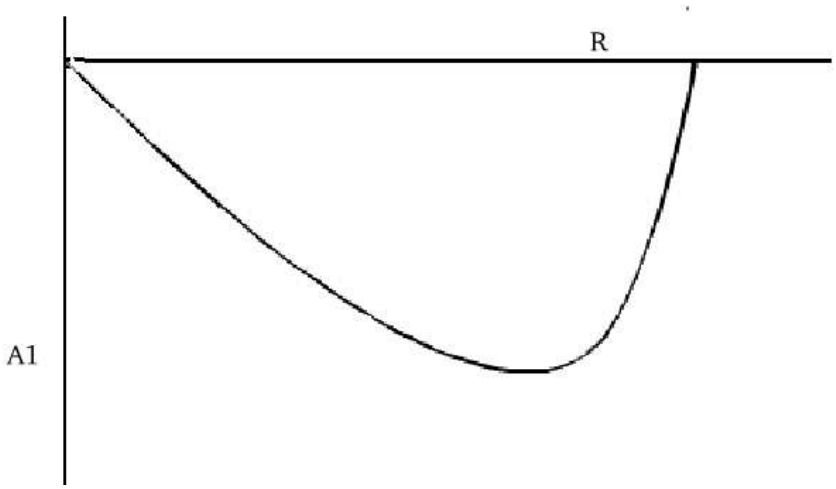

Figure 2.2.2: The heteroclinic connecting the outer stable solution with the rest state. This heteroclinic corresponds to a wave for equation (2.39) with $\epsilon = 0$. The horizontal axis is R and the vertical axis is A_1. In this figure $\hat{J}(k) = 1/(1+k^2)$, $\lambda = -0.5$, $c = 3$ and $\eta = 3.884$.

2.2.3 Waves with a Phase Gradient

Because there is a stable (translation invariant) traveling wave for the case $q = 0$, we suspect that there are waves for values of q in some interval surrounding zero. The major difference in the $q = 0$ waves from the waves with $q \neq 0$ is that a phase gradient is created in the latter.

We will no longer assume that the waves are of a constant velocity. For the remainder of this chapter, a wave (right moving) is a solution such that

$$\lim_{t\to\infty} z(x + At, t) = \rho e^{\imath(\Omega t - kx)} \tag{2.41}$$

for some $A > 0$. The right hand side is the stable plane wave. On the other hand, there is no wave if the condition

$$\lim_{t\to\infty} z(x + At, t) = 0 \tag{2.42}$$

holds for all $A > 0$. These definitions allow for waves that propagate and then recede, but after a number of iterations the front has made progress across the medium. When discussing wave speed we are referring to average wave speed and details regarding calculations of wave speed will be presented whenever relevant. Solutions that appear (numerically) to satisfy (2.42) are discussed in section 2.2.4.

In this section we look at numerical simulations of the waves for small, positive values of q. The characteristics of interest are the wave speed (or average wave speed) as a function of q, and the corresponding phase gradient. We expect that the phase gradient along the wave front increases, in absolute value, as q. We hypothesize that nonzero phase gradients result in slowed waves, relative to the $q = 0$ case.

Consider equation (2.37). The parameter q controls to what extent the amplitude of oscillations at a given x will influence the evolution of θ at x. Since the amplitude of the oscillations are greater once the wave has passed than before it passes, oscillations behind the wave will have a shorter period than those in front. Thus, for any nonzero value of q, a phase gradient will appear. This, in turn, affects the evolution of the amplitude of oscillations. Recall the coupling in equation (2.36):

$$\int J(x-y)[(r^3(y) + \epsilon r(y)) \cos(\theta(y) - \theta(x))]dy$$

When the phase gradient is non zero the $\cos(\theta(y) - \theta(x))$ decreases from 1. This reduces the effective strength of the coupling along the wave front. Because the coupling strength is reduced from the $q = 0$ case, we expect that wave solutions will have lower wave speeds.

At this time it is important to note that we offer no proof of existence for these waves. Although it is likely that the waves for the $q = 0$ case are hyperbolic, in the sense that

small perturbations to a parameter will not result in either destabilization or cessation of existence, we cannot show this explicitly. Instead we rely on the condition

$$c > 2\sqrt{-\lambda - \epsilon c}$$

Recall that this condition was derived using synchronous oscillations of the network, or a zero phase gradient. We claim that the action of the parameter q is to induce a phase gradient along the wave front. As discussed above, this phase gradient results in a lowering of the effective coupling strength. We write

$$R_t = \lambda R - R^5 + c(q) \int_{\mathbb{R}} J(x-y) \left(R(y)^3 + \epsilon R(y) \right) dy \tag{2.43}$$

where $\frac{dc(q)}{dq} < 0$ for every $q > 0$. In addition, $c(0) = c$, the parameter value. If we assume continuity for the function $c(q)$ for small values of q, then we may conclude that the outer periodic solution exists for small values of q and that it is stable, provided that

$$c(q) > 2\sqrt{-\lambda - \epsilon c(q)}$$

Assuming this condition, Chen's Theorem 1 provides the machinery to prove the existence and stability of a traveling wave solution to equation (2.43) for q small.

Simulations support these arguments. For q small the waves propagate across the medium. The wave speed with respect to q is plotted in Figure 2.2.3. For the lesser values of q tested, the curve is rather flat. This is not surprising because the cosine function is flat when the argument is near zero and so the effective coupling strength is relatively insensitive to small phase gradients. For larger q, the slope of the curve decreases from zero. Near $q = 1.2$ the curve is almost vertical. Reliable data for values of $q > 1.2$ were not obtainable.

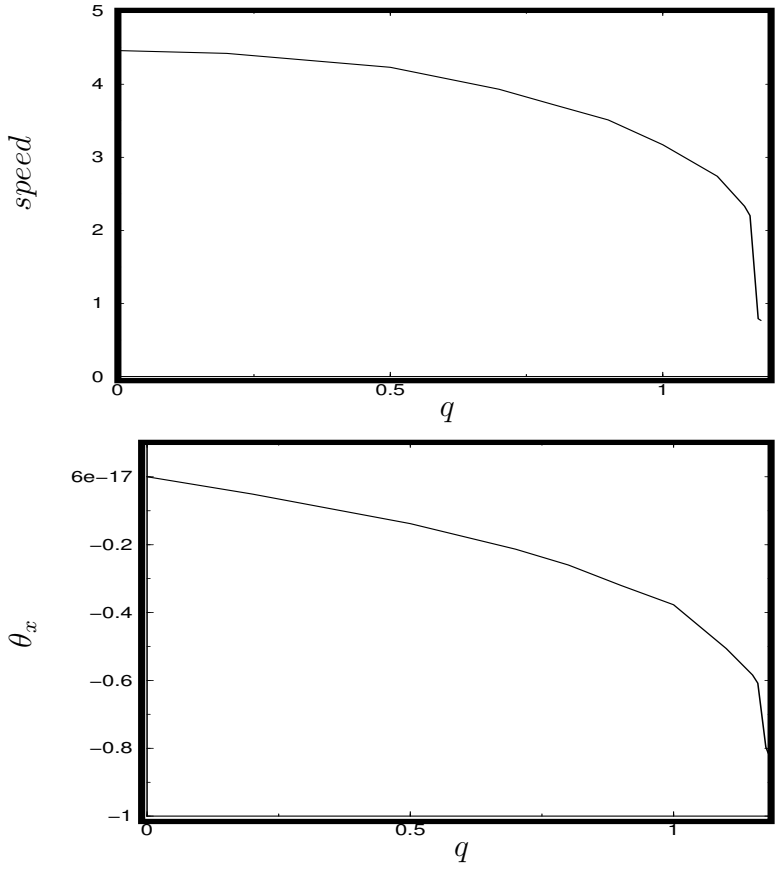

Figure 2.2.3: **Top Panel:** The wave speed as a function of q. The left of the medium was initially excited. The wave speed was calculated by taking the time (from $t = 0$) that $R(40) = 1.5$ and the time that $R(60) = 1.5$ and subtracting. The velocity shown is $20/\Delta t$. **Bottom Panel:** The phase gradient at the wavefront as a function of q. The approximation of the phase gradient was calculated by taking $\theta(61) - \theta(60)$ when $R(60) = 1.5$.

In the lower panel of figure 2.2.3 is a graph of the phase gradient along the wave front. As expected, the phase gradient is an increasing (in absolute value) function of q.

Let $r(x,t,q)$ be the profile of the amplitude of a solution to (2.5). Define the set

$$W = \left\{ q \,|\, \lim_{t\to\infty} r(x+At,t,q) = \rho \text{ for some } A > 0 \right\}$$

If $q \in W$ there is a solution to (2.5) that satisfies (2.41). Numerical simulation of the network suggest that this set is bounded above and there is a critical value

$$q^* = \sup W$$

Figure 2.2.4 shows an example of a wave for $q \in W$, in this case $q = 1$. In the next section we discuss solutions for $q > q^*$.

2.2.4 Localized Regions of Activity

In the previous section, the mechanism by which waves have reduced speed due to a nonzero phase gradient is discussed. This mechanism can be extended to explain solutions that do not propagate across the medium, but are persistent where excitation has already taken place.

It is this type of solution that provides the physiological motivation for this chapter, the behavior of a slice of disinhibited cortical tissue [26, 11]. Shocking the tissue results in a traveling front. Eventually, this front terminates and a pulse results. In addition, stationary patterns of activity in networks has been suggested as a mechanism to model working memory [39, 50]

The network that we are analyzing is a type II network where the threshold is an unstable periodic solution. A similar study for the case of type I networks is presented in [47]. In

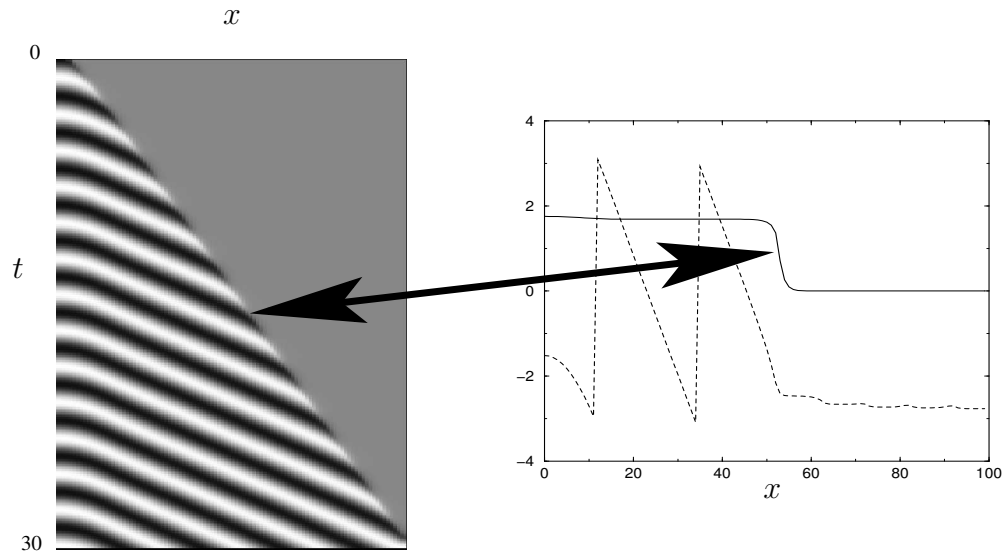

Figure 2.2.4: Traveling wave solution with a nonzero phase gradient. In the left panel the grayscale represents the value of the real component of the variable z. The vertical axis is time and increases in the downward direction. The horizontal axis is space. The value of the real part of z is indicated by greyscale. The right panel is the profile of the amplitude of the system along the domain ($\sqrt{|z|}$, dotted line) and the value of $\theta(x)$ (dashed line). The horizontal axis is the spatial variable, x. The arrow shows the time on the array plot that correspond to the front shown. Parameters for this figure are $\lambda = -0.5$, $c = 3$ and $q = 1$.

this paper, the authors consider a network of type I oscillators connected with excitatory coupling. They show that, in general, propagation will occur if the network is sufficiently synchronous. Asynchrony results in localized persistent activity, where excited locations do not propagate because the overall push to nodes on the edge of the bump is not strong enough for them to exceed threshold. The case that we present here is similar. The amount of synchrony in our network can be quantified by the phase gradient along the real line. When the phase gradient is zero, the oscillators are perfectly synchronized and propagation occurs. This is the $q = 0$ case. When the network is sufficiently desynchronized, given by a large phase gradient resulting from a large value of q, propagation cannot occur and the result is a bump. For the type II case that we study, this is a result of effective lateral inhibition.

Our coupling function, $J(x)$ is positive everywhere. This implies that the coupling is purely excitatory. Normally, an excitatory network is not expected to demonstrate localized regions of persistent activity. On the other hand, using a Mexican hat type interaction function, or a function that satisfies

$$J(x) > 0 \quad \text{when} \quad x \in (a, b)$$
$$J(x) \leq 0 \quad \text{when} \quad x \notin (a, b)$$

easily results in local excitation [1, 27]. The lateral inhibition characteristic of the coupling function causes spacial locations away from the center of the excited state to be inhibited by it, and so they remain near a rest state.

Though our coupling function is non-negative everywhere, the phase gradient caused by non zero values of q induces a lateral inhibition-like effect on the network. Once again, the

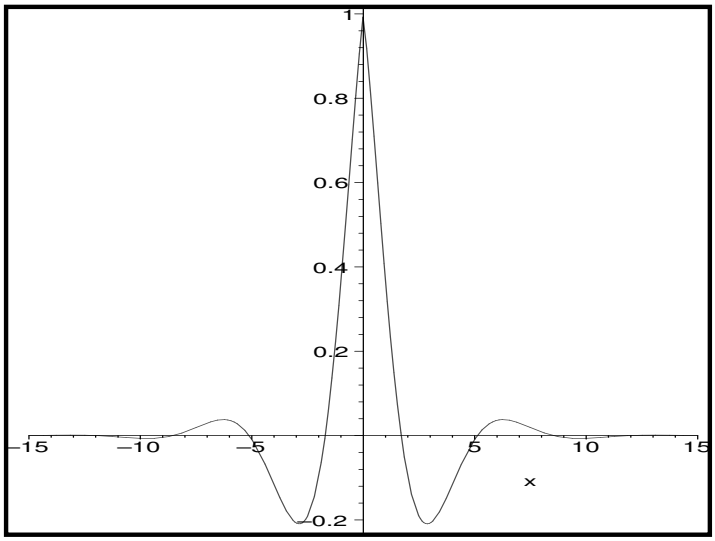

Figure 2.2.5: The interaction function, similar to a Mexican hat. Networks coupled with this type of function often admit persistent localized activity.

coupling term for the evolution of the amplitude of z is

$$\int J(x-y)r^3(y)\cos(\theta(y)-\theta(x))dy \tag{2.44}$$

Let $k(q)$ be the phase gradient at excited regions, such as behind a wave as in figure 2.2.4. We know that this is an increasing function of q. Approximate (2.44) by

$$\int J(x-y)r^3(y)\cos(k(q)(y-x))$$

and rewrite as

$$\int \hat{J}(x-y)r^3(y)dy$$

where $\hat{J}(x) = J(x)\cos(k(q)x)$. This kernel induces lateral inhibition for any phase gradient. A graph this interaction function is shown in figure 2.2.5. As q increases, causing $k(q)$ to

increase, the point on the x-axis where the lateral inhibition begins is closer to $x = 0$. Because $J(x)$ is monotone decreasing as x increases, an increase in $k(q)$ results in stronger lateral inhibition, and less excitation. We hypothesize that some $k^* = k(q^*)$ acts as a threshold such that for $q > q^*$ the lateral inhibition is sufficiently strong to prevent wave propagation. For $q < q^*$ the wave propagates, as in the previous section.

In order to support this numerically we use initial conditions such that the left half line is initially in the excited state, oscillating near the plane wave solution, while the right half line is initially at rest. Figure 2.2.6 shows an array plot of a solution that does not propagate, along with the profile of the function $r(x)$.

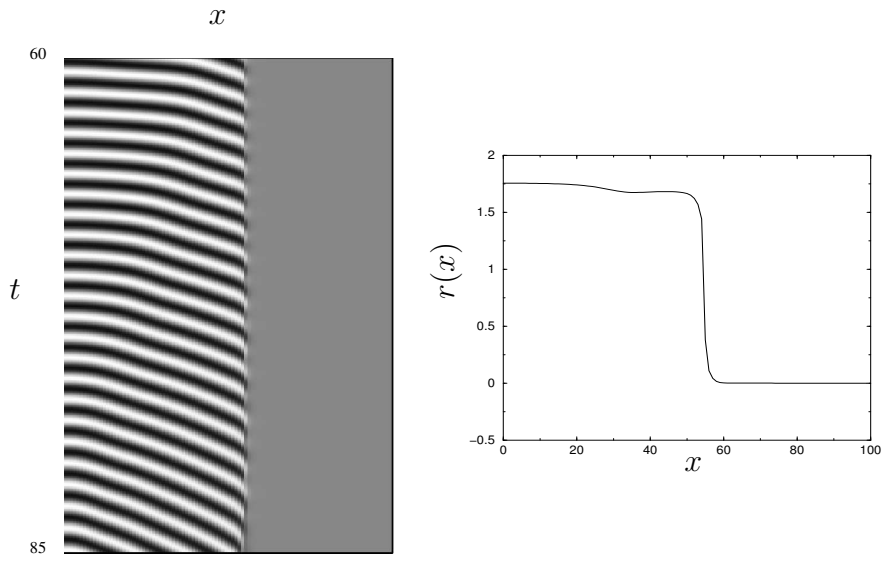

Figure 2.2.6: A solution that does not propagate. The left half line is excited initially and the right half line is initially at rest. The solution propagates slightly but does not cross the entire medium. Parameter values for this solution are $\lambda = -0.5$, $c = 3$, and $q = 2.0$.

We consider the state of the coupling for the solution shown in figure 2.2.6. Figure 2.2.7

shows the value of the function

$$J(x_0 - x)\cos(\theta(x_0) - \theta(x))r(x)^3$$

for $x_0 = 58$. It is easily seen from this figure that the front will not propagate since locations

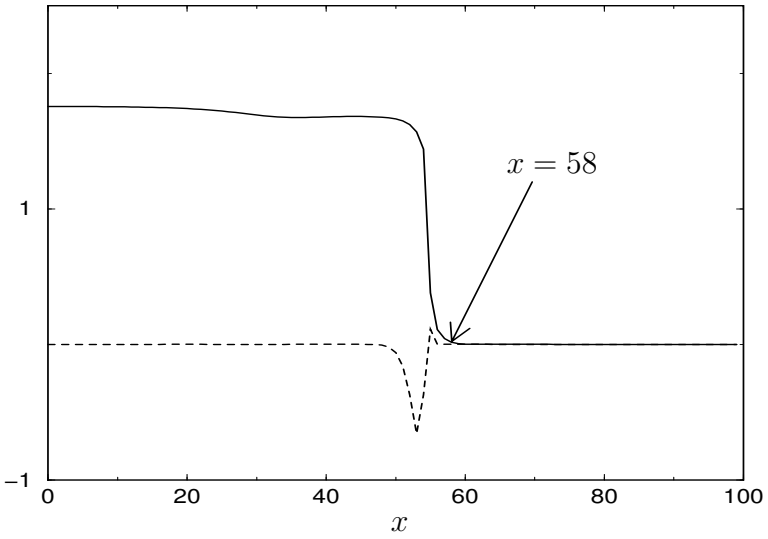

Figure 2.2.7: The state of the coupling for $x_0 = 58$. The solid line is the profile of $r(x)$. The dotted line is the value of the function $J(58 - x)\cos(\theta(58) - \theta(x))r(x)^3$. This function is scaled so that it can be viewed on the same set of axis as r. The figure shows that locations that need to be recruited in order for propagation are actually inhibited by the large amplitude oscillations behind the front.

to the right are inhibited by the already excited region.

The mechanism responsible for localized regions of persistent activity is identical. The initially excited region need not span the entire half line. As long as the interval of initial excitation is large enough that it can sustain itself oscillations will persist. The lateral inhibition prevents propagation on both fronts. A bump for $q = 2$ is shown in figure 2.2.8.

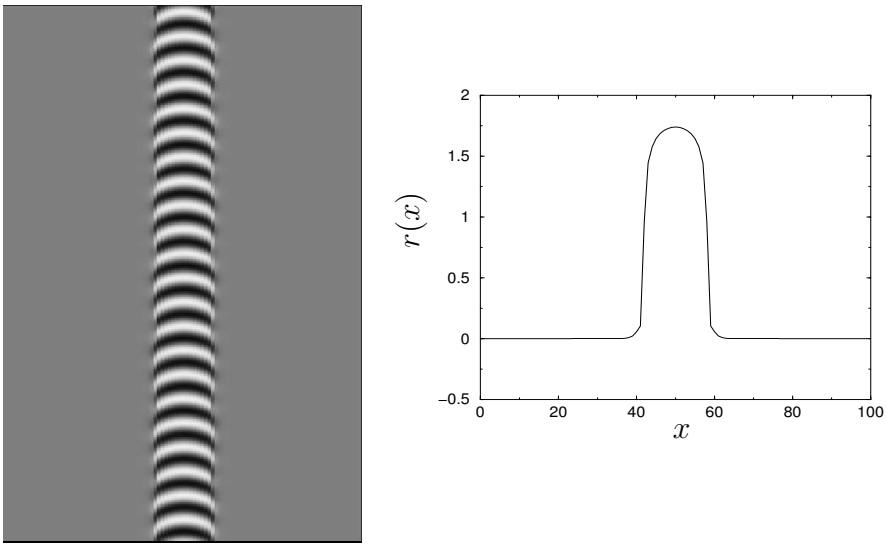

Figure 2.2.8: A persistent pulse. On the bump the oscillations remain near the plane wave solution. On either side of the bump, the oscillations are inhibited via the lateral inhibition mechanism discussed. The right panel shows the profile of the bump at a fixed time. The parameter values for this figure are $\lambda = -0.5$, $c = 3$ and $q = 2$.

The pulses will not, in general, have stationary profiles satisfying

$$0 = \lambda R - R^5 + c \int_{\mathbb{R}} J(x-y)\cos(\theta(x) - \theta(y))R(y)^3 dy$$

The evolution of the phase of oscillators on a pulse will be faster than the corresponding evolution of oscillations away from the pulse. Suppose there is a pulse solution centered at $x = 0$. As $x \to \infty$ the period of oscillations decreases to zero. On the other hand, the center of the pulse has $\frac{\partial \theta}{\partial x} \approx 0$ and so the coupling is small. This allows the approximation

$$\frac{\partial \theta}{\partial t} \approx qr(x)^2$$

This implies periodicity in the value

$$(\theta(0) - \theta(x)) mod(2\pi)$$

for x sufficiently far from zero. This, in turn, results in periodic strength of coupling. The coupling alternately inhibits and excites locations on the sides of the bump. This is the motivation for the definitions (2.41) and (2.42). The front locates so that the net effect of the alternating excitation and inhibition is zero. Figure 2.2.9 shows the minimum and maximum, determined as closely as possible, of a bump. In figure 2.2.7 the configuration shown is during the time when the bump is receding.

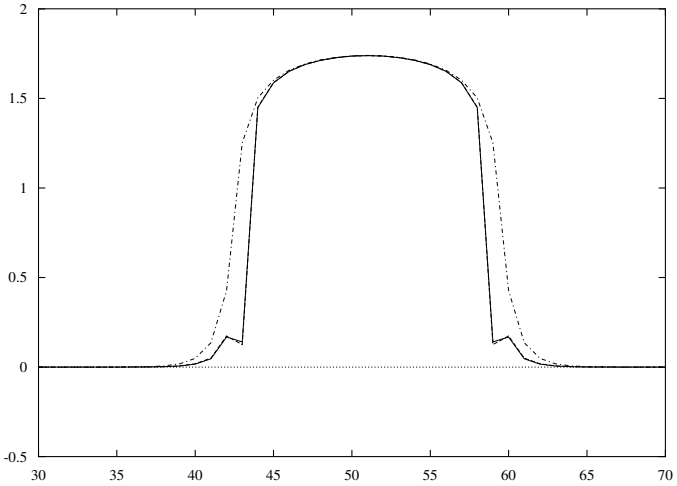

Figure 2.2.9: A breathing pulse. Each curve shows the profile of the amplitude. The solid curve is the minimum state of the breather, as well as could be determined. The dotted curve is the maximum state. The profile oscillates between these two states. For this figure $\lambda = -0.5$, $c = 3$ and $q = 2$.

2.3 SUMMARY

In this chapter we discuss solutions to an evolution equation where the uncoupled system is near a degenerate Hopf bifurcation. Without coupling, all solutions go to the rest state. The coupling that we use is chosen so that the degeneracy is removed and the stability properties of the rest state are unaffected. Also, the coupling is purely excitatory, so that oscillations get a push from nearby activity.

We obtain useful conditions on the parameters by analyzing a two equation model that possesses the important characteristics of the full equation. Under these conditions we are able to prove the existence and linear stability of plane wave solutions bounded away from rest. The configuration is a branch of unstable periodic solutions that turns around to form an outer branch of stable periodic solutions.

We prove the existence and stability of traveling waves for the case where zero phase gradients are time invariant. For the case where phase gradients occur we describe a lateral inhibition mechanism by which waves continue to exist but with slower wave speeds. Finally, we show that the when the network is sufficiently desynchronized the lateral inhibition effect is strong enough to prevent propagation. The resulting Mexican hat-like interaction allows regions of persistent activity. These pulses are not stationary bumps. The profile of the bumps alternately advances and retreats so that the net propagation is zero.

3.0 LOW FIRING FREQUENCY FOR A NETWORK OF HODGKIN-HUXLEY NEURONS WITH EXCITATORY SYNAPTIC COUPLING

In this chapter we explore a phenomena in the Hodgkin-Huxley model of the squid giant axon [32]. Similar to the previous chapter, this problem involves unusual implications of excitatory coupling. The focus of this chapter is the exploration and analysis of a subtle mechanism that causes the network to synchronize rapidly and fire slowly.

The individual cells that we study are of type II excitability, as in the previous chapter. We consider the case where each cell received sufficient applied current to sustain firing in the absence of coupling. When coupled, the network rapidly synchronizes. Once synchronized the network continues to fire since the applied current is superthreshold. The unusual effect is that the synchronized network fires much more slowly, or has longer interspike intervals (ISIs) than the uncoupled network. We show that this is the result of an interesting mathematical structure called a canard. In two dimensions canards are rather delicate and are often only realized in the context of canard explosions [15]. In three dimensions a canard is somewhat less sensitive to perturbations in the parameters [52], and this case is no exception. The mechanism that we describe is very robust and exists over a large interval of parameter values.

Large ISIs in the Hodgkin-Huxley neuronal model have been explored previously in [19]. Unlike what we explore, the authors numerically analyze an uncoupled cell. The authors decomposed the system into slow and fast components and changed the values of τ_n and τ_h, the timescales of evolution for the n and h variables. The slowing of the network was attributed to a lowering of the instability (decrease in the real part of the eigenvalues) of a critical point in the fast subsystem. The vortex structure that we present in this work was not discovered.

Also, in [48] it is shown that synchronized relaxation oscillations can exhibit a longer period than the corresponding uncoupled system. In [29] it is shown how weakly coupled oscillations can exhibit lower firing frequencies once synchronized. Each of these works are summarized in [46]. The phenomena that we explore takes place entirely in the silent phase, unlike the case in [48]. Also, we are not under the weak coupling assumption. The mechanism that we explore is not of either of these types.

The structure of this chapter is as follows:

- We show, via simulation, the effect of the coupling for a network of Hodgkin-Huxley neurons. We show that the same effect is present for a reduced model, obtained as in [45]. Finally, due to synchrony, we justify the use of a self coupled model to approximate the behavior of the full system.
- We propose a simple model that has all of the necessary ingredients for the slowing.
- We approximate the difference between two calculations of the slow passage, or equivalently, the release value for the synaptic variable. To this end, we employ slow passage calculations through a Hopf bifurcation [4, 41, 42] to obtain a way-in way-out function that relates the strength of the attraction before the bifurcation to the strength of

repulsion after the orbit has passed.

3.1 NUMERICAL SIMULATIONS OF NETWORKS

A network of excitatory cells has, in general, well known behavior. The effect of excitatory coupling on synchrony is of particular importance here. There are a number of factors, but we focus on properties of the intrinsic dynamics of an individual neuron. If a neuron is of type I excitability (a saddle node configuration), excitatory coupling typically desynchronizes a network [25]. For a type II neuron (large amplitude periodic solutions are the result of a Hopf bifurcation) excitatory coupling typically causes the network to synchronize [30]. For the network we consider fast threshold modulation [48] plays a role in the rapid synchronization.

Figure 3.1.1 shows one example of each of these configurations. In the left panel of the figure a network of Traub pyramidal neurons is shown [49]. These neurons are type I excitable. Also, the applied current is sub threshold and thus will not cause the network to ignite at any location without receiving excitation from other other cells in the network. Readily seen in the figure is rapid, asynchronous firing. This is often the case when excitable neurons are coupled together [30, 31, 28], and in particular type I [25]. The right panel depicts the behavior of a network of Hodgkin-Huxley neurons, which are type II excitable. The applied current for this simulation is above threshold and so, even in the absence of coupling, the individual neurons will oscillate. As the excitatory coupling is introduced the network rapidly synchronizes and the interspike intervals increase.

The goal of this chapter is to explain the extreme slowing of firing in the Hodgkin-Huxley

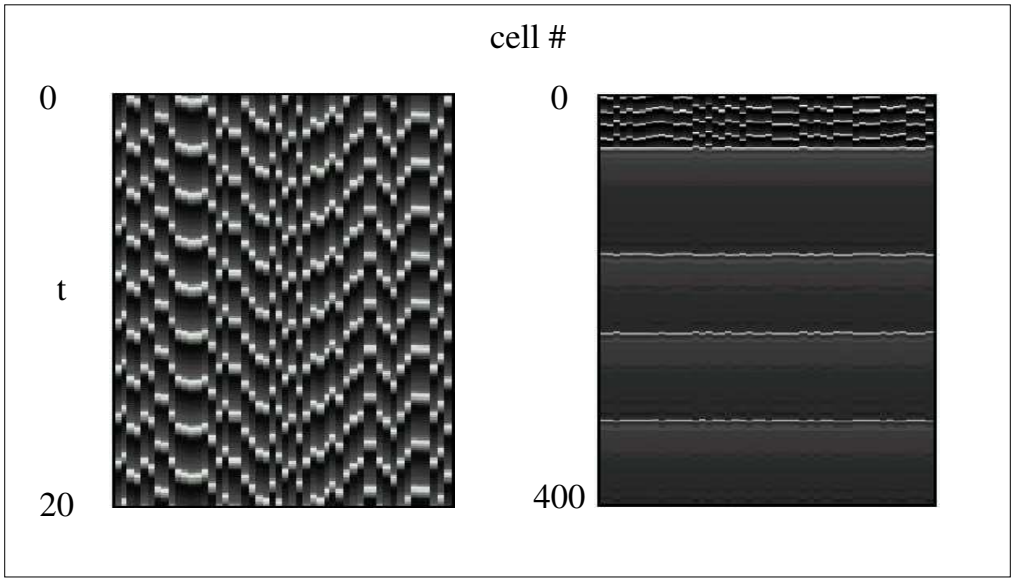

Figure 3.1.1: Behavior of networks of neurons coupled with excitatory coupling depends on the intrinsic dynamics. The left panel shows the activity of 50 cells with Traub pyramidal cell dynamics. The type 1 neurons do not synchronize and maintain activity with a subthreshold applied current. The right panel is 50 Hodgkin-Huxley neurons. These neurons reach near synchrony (spikes, though subthreshold oscillations may be out of phase) once the coupling is turned on. The current applied here is superthreshold, though the ISI is somewhat longer than for the uncoupled system.

network. We begin by reducing the full HH system to a lower dimensional system, using well known techniques [45]. The reduced system behaves similarly to the full system. The only difference is that in the reduced model the sub threshold oscillations that lead up to a jump to the large amplitude periodic are synchronized, while in the full model they are not. The reduced system is given by

$$\begin{aligned} C\tfrac{dV}{dt} = & \; -g_L(V-V_L) - g_K n^4(V-V_K) - g_{Na} m^3 h(V-V_{Na}) \\ & +I_0 - g_{syn} s(V-V_{syn}) \\ \tfrac{dh}{dt} = & \; \tfrac{h_\infty(V)-h}{\tau_h(V)} \\ m = & \; m_\infty(V) \\ \tfrac{ds}{dt} = & \; \alpha(V)(1-s) - \tfrac{s}{\tau_{syn}} \end{aligned} \tag{3.1}$$

The values of the parameters and the various functions are given in the appendix. The self coupling in this model is used to make analysis simpler by only observing a single cell while emulating the behavior of the entire network. The rapid synchronization of the coupled network justifies this simplification.

3.2 THE V-H PLANE

We rewrite the equations for the reduced HH model (3.1)

$$C\frac{dV}{dt} = f(V,h) - g_{syn} s(V-V_{syn}) \tag{3.2}$$

$$\frac{dh}{dt} = \alpha_h(V)(1-h) - \beta_h(V)h \tag{3.3}$$

where

$$f(V,h) = I_0 - g_{Na}h(V - V_{Na})m_\infty^3(V) - g_K(V - V_k)n^4(h) - g_l(V - V_l)$$

and the equation for the synapse is

$$\frac{ds}{dt} = \alpha(V)(1 - s) - \frac{s}{\tau_{syn}} \tag{3.4}$$

In this section we observe the behavior of the system of equations (3.2), (3.3) with the value of s fixed, as if it were a parameter.

For our parameter values, the variable h evolves more slowly than V. The behavior of the $V - h$ system depends on the value of s. If s is large then there is a stable fixed point at the intersection of nullclines and therefore no oscillations. For s small enough the fixed point is no longer stable and there is a large amplitude periodic. The transition between these states is a Hopf bifurcation (figure 3.2.1).

For each value of fixed s the set of solutions to $\frac{dV}{dt} = 0$ forms a triple branched curve. The outer branches are attracting. For values of s corresponding to an unstable fixed point the periodic can be decomposed into a silent phase (trajectory is near the curve $\frac{dV}{dt}$) and an active phase. This is a relaxation oscillation where the trajectory follows a critical manifold until reaching a fold. Once the trajectory reaches the fold, the fast variable dominates and there is a jump to the other stable branch of the fast nullcline (figure 3.2.2).

The slowing mechanism that we discuss takes place during the silent phase, or the period of time that the trajectory is near the left branch of the V-nullcline. During this time, the function $\alpha(V) \approx 0$ and so we get that

$$\frac{ds}{dt} \approx -\frac{s}{\tau_{syn}}$$

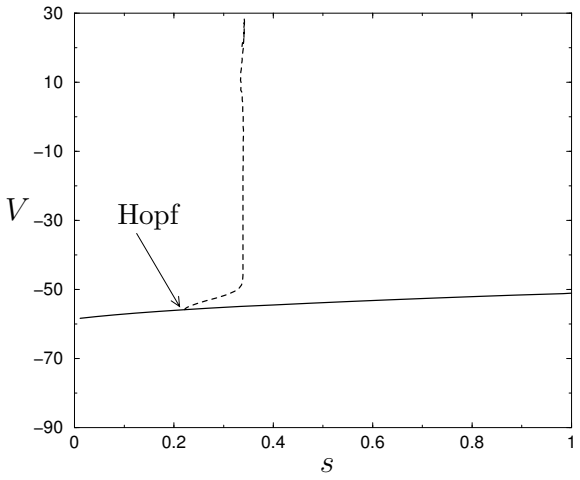

Figure 3.2.1: Bifurcation Diagram for the HH equations parameterized by s. As s decays the attractor during the silent phase changes stability via a Hopf bifurcation. For values of s to the right of the bifurcation point the steady state solution is stable. For values of s to the left the fixed point is unstable. This bifurcation results in the large amplitude periodic solutions corresponding to spikes, which are difficult to obtain with any accuracy numerically and omitted.

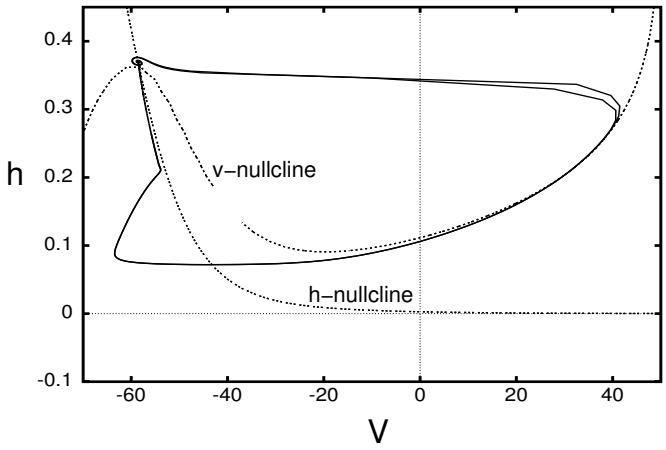

Figure 3.2.2: The projection of the system (3.2)- (3.4) onto the $V - h$ plane. The trajectory travels up the fast nullcline as s decays in the left plane. Eventually the trajectory escapes and jumps to the other branch of the fast nullcline and repeats. The fast nullcline is only shown for a small value of s, near the release point. For larger s, the nullcline is lower in the h direction and raises up as s decays.

The V-nullcline depends on s and will move up in the h direction as s decays. The h-nullcline does not depend on s. Though much of our analysis is based on the $s' = 0$ case, it is important to note that s evolves whenever V and h do.

3.3 THE INTERSECTION OF NULLCLINES AND EXTENDED DELAY

For s large and fixed the intersection of the nullclines corresponds to a stable equilibrium point for the system. As s decays through the interval of s values corresponding to a stable equilibrium the trajectory is drawn towards the intersection. As s decays past the value that is associated with the Hopf bifurcation, the trajectory continues to approach the intersection. When s gets very small there is an escape to the large amplitude oscillation, or spike. From simulations alone, one would estimate that the bifurcation value for fixed s is quite small, but this is not the case. As seen in figure 3.2.1, the bifurcation value is $s \approx 0.222$, while the escape takes place for a much smaller value. This implies that the orbit is drawn toward the intersection even as it represents an unstable equilibrium. The goal of the remainder of this section is to uncover the mechanism by which this occurs, and to use this mechanism to develop an expression that gives an estimate of the value of s that corresponds to escape and hence an estimate of the duration of this delay.

3.4 INGREDIENTS FOR THE DELAY

In the system (3.2), (3.3), (3.4) orbits appear to be attracted to a point that is unstable for the case of s fixed. For the full system, where s decays exponentially, there are no equilibrium

points for $s > 0$. Linear stability results based on the fixed s analysis may not apply here, and the curve of values in the $V - h$ plane may not repel the orbit when it is unstable for the fixed s system. Linear stability results may not be suitable for this problem.

There are a number of candidates for the cause of this delay. The simplest to visualize is that the h-nullcline has negative slope with respect to V during the silent phase. Also, the point $(V(t), h(t))$ lies to the left of this nullcline and so h is increasing. As s decays, the h values along the V-nullcline are increasing, and so the intersection is moving up and left in the $V - h$ plane. This provides a mechanism for the decay of s to drive the orbit towards the intersection regardless of the linearization about the intersection.

For a value of s near the Hopf bifurcation, the nullclines are in the fold canard configuration [15]. Although this only lasts for a small interval of time it may provide the mechanism for a canard to arise in the full system. It must be noted at this point that we will not utilize tools such as nonstandard analysis or a singular decomposition of the slow and fast components of the system, though this canard configuration appears to be quite important in any system that exhibits this delay.

3.5 A SIMPLE SYSTEM

In order to do any direct analysis on the slowing mechanism it is ideal to have a system that is simpler than the system defined by (3.2)- (3.4). We want a system where the right hand sides are polynomials in the variables so that the nullclines are given by polynomials. We wish for our model to incorporate the following characteristics:

- The slow nullcline has a negative slope with respect to the fast variable, provided the

trajectory approaches the slow nullcline from the left after it enters the silent phase. If the approach is from the right, then we require that the slope of the nullcline be positive.

- When parameterized by s, we require that the eigenvalues of the linearization at the intersection of the nullclines be positive for large values of s, and then change stability via Hopf bifurcation as s decays. For values of s near the bifurcation value the system must be in the fold canard configuration.
- The vector field of the system is analytic and autonomous during the silent phase.

The model that we use to incorporate these items is

$$\frac{dx}{dt} = -f(x) + y - I(s)x \tag{3.5}$$

$$\frac{dy}{dt} = -\epsilon\left(y + \frac{1}{4}x^5\right) \tag{3.6}$$

$$\frac{ds}{dt} = -\frac{s}{\tau_{syn}} \tag{3.7}$$

where $0 < \epsilon \ll 1$. We only consider $x < 0$ since the behavior during the active phase does not effect the behavior during the silent phase besides resetting the configuration after a spike. The functions in the simple system are given as

$$f(x) = \frac{1}{4}x^3 - 2x$$

and

$$I(s) = \frac{3}{2}s.$$

3.5.1 Notation

We use the following notation for the remainder of the chapter:

- $N_f(x,s) : \mathbb{R}^2 \to \mathbb{R}$ is the y-coordinate of the fast nullcline ($\{y|\frac{dx}{dt}(x,y,s) = 0\}$). This function is well defined for each point $(x,s) \in (-\infty, 0) \times [0,1]$.
- $N_s(x) : \mathbb{R} \to \mathbb{R}$ is the y-coordinate of the slow nullcline ($\{y|\frac{dy}{dt}(x,y) = 0\}$). This function is also well defined for all $x < 0$. Note that there is no s dependence.

These curves are given by

$$N_f(x,s) = f(x) + I(s)x$$

$$N_s(x) = -\frac{1}{4}x^5$$

We have that $\frac{\partial N_f}{\partial s} < 0$ for $x < 0$ and these curves intersect for each fixed s. We let $(\tilde{x}(s), \tilde{y}(s))$ denote the curve of intersection points.

3.6 ANALYSIS USING THE VARIATIONAL EQUATION

In this section we describe the method that we use to approximate the release value of s. Consider a system

$$x' = f(x,y)$$

$$y' = g(x,y).$$

Suppose that there is a curve in the $x - y$ plane, G, that acts as and attractor for certain values of x and y, and then switches to a repelling curve after the solution crosses some threshold. We can approximate the behavior in a neighborhood of this curve by using a

variational equation

$$\frac{d}{dt}\begin{pmatrix} z_1 \\ \\ z_2 \end{pmatrix} = A(G)\begin{pmatrix} z_1 \\ \\ z_2 \end{pmatrix} \tag{3.8}$$

where

$$A(G) = \begin{pmatrix} \frac{\partial f}{\partial x}(G) & \frac{\partial f}{\partial y}(G) \\ \\ \frac{\partial g}{\partial x}(G) & \frac{\partial g}{\partial y}(G) \end{pmatrix}$$

The solution to equation (3.8) can be written

$$\begin{pmatrix} z_1 \\ \\ z_2 \end{pmatrix} = \exp\left(\int_0^t A(G(s))ds\right)\begin{pmatrix} z_{10} \\ \\ z_{20} \end{pmatrix}$$

where $z_1(t) = x - G_1$ and $z_2(t) = y - G_2$. The functions G_1 and G_2 are the x and y component of G, respectively. This solution can be used to approximate the solution to the full system in a neighborhood of G. In this paper, we use it to approximate the value of the independent variable when the solution leaves a specified neighborhood of the curve. Our method is described here.

We use the 2-norm. Choose an entrance criterion, η, the value of the initial distance of the solution from the curve for the initial value of the independent variable. For the example above, we choose $t = 0$ and a value of (x, y) such that $\|(z_1(t), z_2(t))\| = \eta$. Since the curve G is assumed to be an attractor at first, the solution to (3.8) will decay for a period of time. Once the attractor switches to a repelling curve, the solution to (3.8) will grow. We look for the first value of t such that

$$\left\|\begin{pmatrix} z_1(t) \\ \\ z_2(t) \end{pmatrix}\right\| = \eta$$

This value of t will be called the release value, or the value of t where the solution is no longer in the specified neighborhood of the curve G.

There are some issues that must be resolved before one can expect this analysis to result in an accurate approximation of the behavior of the full system. Consider the example discussed in [15]

$$\epsilon x'' + (x' + a) + x = 0$$

where $a = 0.0000001$. If we rewrite as

$$x' = y = f(x, y)$$

$$\epsilon y' = -x - (a + y)^2 = g(x, y)$$

we can view the system on the phase plane, as in figure 3.6.1 In [15], the domain of the way-in way-out function (equivalent to our variational equation) is determined by the location of a funnel, a curve in the plane where solutions leave a neighborhood of the critical manifold together (see figure 3.6.1). For trajectories that enter the desired neighborhood of the critical manifold to the right of the funnel, the way-in way-out function will give good approximations. However, because our variational equation is just a decaying exponential during the attracting phase and a growing exponential during the repelling stage, the results for initial entry to the left of the funnel will give misleading information. The variational approximation will always give longer release times for longer attracting times. This is inconsistent with the actual results, where there is an upper bound for release times, caused by the funnel. The domain of the way-in way-out function is only those entry locations that are unaffected by the funnel.

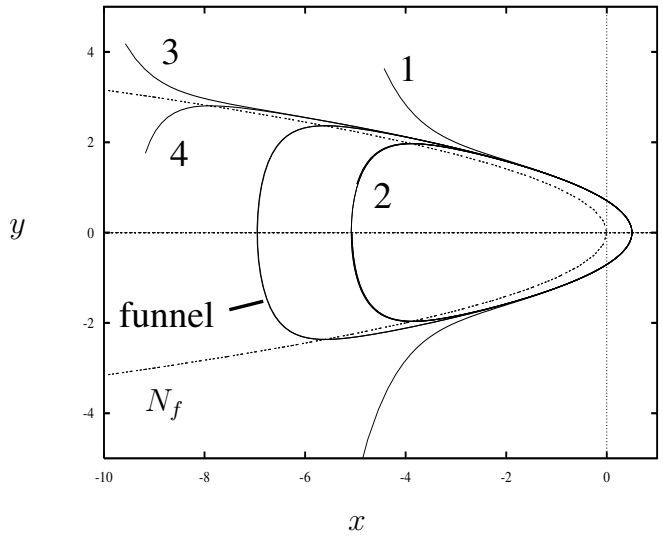

Figure 3.6.1: A trajectory funnel. The equation represented here is $x'' + (x' + a)^2 + x = 0$. The x-nullcline is marked N_f and the y-nullcline lies on the x-axis. Trajectories 1 and 2 are candidates for a variational approach. Trajectories 3 and 4 are not, since they each leave some neighborhood of the critical curve at roughly the same location.

For our problem, we must locate the domain of our way-in way-out function. We do this by plotting the value of s_{exit} as a function of s_{enter} for actual solutions (Figure 3.6.2). For entry values of s located within the domain of our way-in way-out function the value of s_{exit} will be a decreasing function of s_{enter}. We assume that the variational approach is invalid for larger values of s_{enter}, where the graph is flat. Figure 3.6.2 suggests the domain of our way-in way-out function can be approximated by the interval $[0.45, 0.55]$. For s larger than 0.55, there is a funnel. For s smaller than 0.45 the trajectory does not spend enough time in the attracting phase and the stays further from the vortex curve. For this situation a linear approximation of the system around the vortex point is inadequate. For analysis in the following sections we will use $s_{enter} = 0.5$.

In the following sections we perform a way-in way-out analysis for two curves. In the next section we do the calculations for the intersection of the nullclines. Following this, we perform the calculations for a different curve that acts as a trapping mechanism. The details of both of these calculations can be found in section 3.11.

3.7 ANALYSIS AROUND THE INTERSECTION OF THE NULLCLINES

In figure 3.2.2 it can be seen that the trajectory is visibly separated from the graph of $N_s(x)$, and hence there is separation from the intersection of the nullclines. This does not rule out the possibility that the variational analysis described in the previous section will give a good approximation to the release value of s. We will perform the analysis, a comparison between the approximation obtained from the above analysis and the actual results, and show that in fact this is not the optimal curve and that the approximations are less than ideal.

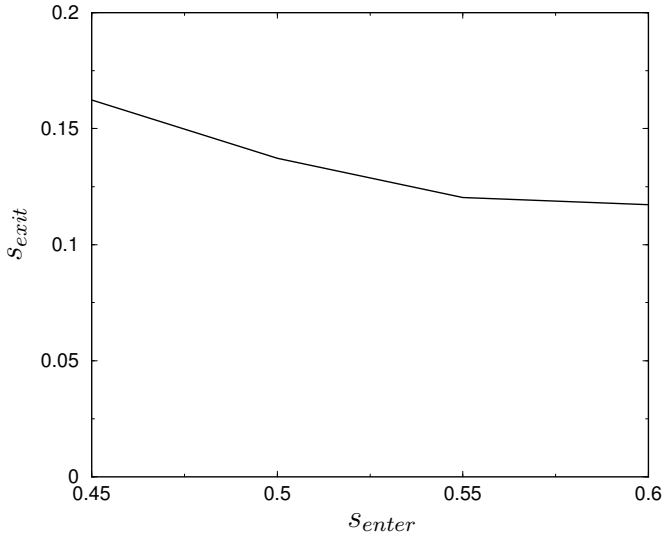

Figure 3.6.2: An approximation to the domain of the way-in way-out function used to approximate the release value of s. To determine the domain of this function, we look for values of s_{enter} such that an increase will result in a decrease in the corresponding value of s_{exit}. For value of s_{enter} greater than those shown the graph is somewhat flat.

We carry out the calculation of the standard method. Let $J(s)$ be the Jacobian matrix of the system defined by (3.5)- (3.6) along the the curve $(\tilde{x}(s), \tilde{y}(s))$. We have that

$$J(s) = \begin{pmatrix} -\frac{3}{4}\tilde{x}^2(s) + 2 - I(s) & 1 \\ -\epsilon\frac{5}{4}\tilde{x}^4(s) & -\epsilon \end{pmatrix} \tag{3.9}$$

The equation of variation is

$$\frac{d}{ds}\begin{pmatrix} x \\ y \end{pmatrix} = -\frac{\tau_{syn}}{s} J(s) \begin{pmatrix} x \\ y \end{pmatrix} \tag{3.10}$$

The solution to (3.10), given an initial value (x_0, y_0, s_{enter}), is

$$\begin{pmatrix} x \\ y \end{pmatrix} = \exp\left(\int_{s_{enter}}^{s} -\frac{\tau_{syn}}{\omega} J(\omega) d\omega\right) \begin{pmatrix} x_0 \\ y_0 \end{pmatrix} \tag{3.11}$$

Given the initial condition we may solve the equation

$$\left\| \exp\left(\int_{s_{enter}}^{s} -\frac{\tau_{syn}}{\omega} J(\omega) d\omega\right) \begin{pmatrix} x_0 \\ y_0 \end{pmatrix} \right\|_2 = \left\| \begin{pmatrix} x_0 \\ y_0 \end{pmatrix} \right\|_2 \tag{3.12}$$

This equation gives an approximation of s such that the distance (in the plane) of the orbit from the intersection is the same as it was when it entered. We take this to be the exit value of s.

For typical slow passage problems [15, 14, 41, 42], the value obtained by solving (3.12) gives a good approximation for the exit value of s. For the problem under consideration here, the results are poor, especially for the lower values of τ_{syn} tested. This is not surprising. When the decay of s is not sufficiently slow compared to the evolution of y, the standard theory breaks down. The results for an interval of τ_{syn} is shown in figure 3.7.1. Solving equation (3.12) results in an overestimate for the release value of s, and a corresponding

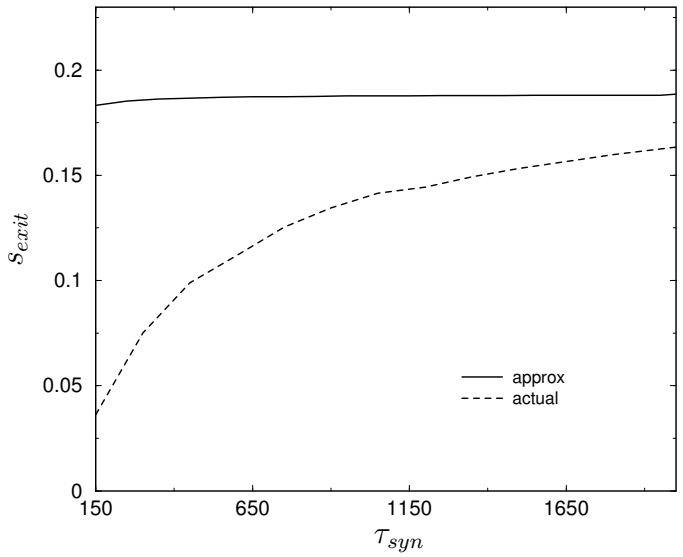

Figure 3.7.1: Comparison between the actual release value for s and the approximation obtained via the variational method. The curve of approximations is somewhat invariant with respect to τ_{syn}. This is expected since the only place that τ_{syn} appears in the variational equation (3.11) is a multiplying constant. To obtain these curves we chose $s_{enter} = 0.5$ for the reasons discussed in the previous section. The initial conditions that we chose are $x_0 = -\eta$ and $y_0 = 0$. For this figure $\eta = 0.3$. The corresponding initial conditions for the actual values obtained are $x_0 = \tilde{x}(s_{enter}) - \eta$ and $y_0 = \tilde{y}(s_{enter})$.

underestimate for the time spent in the silent phase. Note also that the curve of approximations in figure 3.7.1 is somewhat flat. This is expected since the Jacobian matrix (3.9) does not depend on τ_{syn}. It does appear in equation (3.11), but this equation can be written

$$\begin{pmatrix} x \\ y \end{pmatrix} = \exp(\tau_{syn}) \exp\left(\int_{s_{enter}}^{s} -\frac{1}{\omega} J(\omega) d\omega \right) \begin{pmatrix} x_0 \\ y_0 \end{pmatrix}$$

And the equation to be solved can be written

$$\left\| \exp\left(\int_{s_{enter}}^{s} -\frac{1}{\omega} J(\omega) d\omega \right) \begin{pmatrix} x_0 \\ y_0 \end{pmatrix} \right\| = \eta \exp(-\tau_{syn})$$

This implies that

$$\frac{d}{d\tau_{syn}} \left\| \exp\left(\int_{s_{enter}}^{s} -\frac{1}{\omega} J(\omega) d\omega \right) \begin{pmatrix} x_0 \\ y_0 \end{pmatrix} \right\| = -\eta \exp(-\tau_{syn})$$

which is small. Since the norm requirement for exit does not depend strongly on τ_{syn}, the value of s that satisfies equation (3.12) will reflect this.

On the other hand, simulations suggest that the value of s that satisfies the exit criterion should vary as the logarithm of τ_{syn}.

The poor performance of the usual slow passage approach suggests that this is not the ideal method for approximating the release value of s, and the corresponding time spent in the silent phase. In the remainder of this chapter we discuss a trapping mechanism (vortex canard) that is also represented as a curve in the $x - y$ plane. We will show that approximations based on the new structure will yield superior results to the usual approach discussed in this section for values of τ_{syn} where the evolution of y and s are on similar time scales. For sufficiently slow synaptic decay (large τ_{syn}) we find that the usual approach is sufficient and as $\tau_{syn} \to \infty$, the approaches are identical.

3.8 THE TRAPPING MECHANISM

As s decays, the function $N_f(x,s)$ will rise for relevant values of $x < 0$ since $\frac{\partial N_f}{\partial s} < 0$. Consider the set

$$A(s) = \{(x_0, y_0) \mid \frac{dy}{dt}(x_0, y_0) < \frac{dN_f}{ds}(x_0, s)\frac{ds}{dt}\} \tag{3.13}$$

This set consists of the points in the $x-y$ plane that are evolving in the y direction more slowly that the fast nullcline evaluated at the same x coordinate. This set is nonempty since $N_f(x,s)$ increases as s decays for fixed $x < 0$. The evolution in the y direction on the slow nullcline is 0, and so the slow nullcline is in the set $A(s)$ for any value of s. Also, as $x \to -\infty$, $\frac{dy}{dt} \to \infty$ and so this set has a left boundary for any value of s. This boundary is a curve in the $x-y$ plane and will be denoted by $y_{\partial A(s)}(x)$. For the simple system (3.5), (3.6) we can express the boundary curve explicitly

$$y_{\partial A(s)}(x) = -\frac{1}{4}x^5 + \frac{3xs}{2\epsilon\tau_{syn}} \tag{3.14}$$

Notice that as $\tau_{syn} \to \infty$ we have that $y_{\partial A(s)}(x) \to N_s(x)$ and that $y_{\partial A(0)}(x) = N_s(x)$.

The boundary curve is shown in figure 3.8.1, along with the nullclines $N_f(x,s)$ and $N_s(x)$. This figure also reveals the trapping mechanism that causes the delay. If the trajectory lies to the right of $y_{\partial A(s)}(x)$ the trajectory will be moving in the positive y direction more slowly than the fast nullcline at the same x coordinate. If the orbit lies above the fast nullcline, it may cross it and begin to move leftward in the plane. The solution then can cross the boundary curve and will begin to evolve in the y direction faster than $N_f(x,s)$. Again, it may cross the fast nullcline and begin to move rightward in the plane eventually crossing the boundary curve. This repeats and the result it a vortex structure that evolves along the

intersection of the boundary curve and the fast nullcline. We aim to show that this structure is, for s above a certain value determined by τ_{syn}, a good approximation to the attractor that causes the long ISIs. It must be restated that this vortex point is only an approximation to the attractor. To explain why we denote the intersection of the curves $N_f(x,s)$ and $y_{\partial A(s)}$ as $(\hat{x}(s), \hat{y}(s))$. Notice that

$$\frac{d\hat{y}(s)}{ds}\frac{ds}{dt} = \frac{\partial N_f}{\partial s}\frac{ds}{dt}$$

is not satisfied. This is because the set definition (3.13) is for fixed x_0. The set $A(s)$ is used only to specify the location of the intersection, not the evolution of it. We need to satisfy the condition

$$\hat{y}(s) = N_f(\hat{x}(s), s)$$

for each value of s. Implicitly differentiating the above expression gives

$$\frac{d\hat{y}}{ds}(s) = \frac{d\hat{x}}{ds}\frac{\partial N_f}{\partial x}(\hat{x}(s), s) + \frac{\partial N_f}{\partial s}(\hat{x}(s), s).$$

The set A was developed using the assumption that $\frac{\partial N_f}{\partial x} \approx 0$. In addition, the actual attractor should be a solution of the system of equations (3.17)- (3.18). This is obviously not the case for our approximation, since the vortex point always lies on the fast nullcline and would correspond to vertical solutions in the plane.

Simulations verify that the actual solution follows the curve of vortex points very closely. In the next section, we perform the linear stability analysis about this curve to determine what values of s result in an attractor, as well as a bifurcation value of s where the vortex structure switches from attracting to repelling.

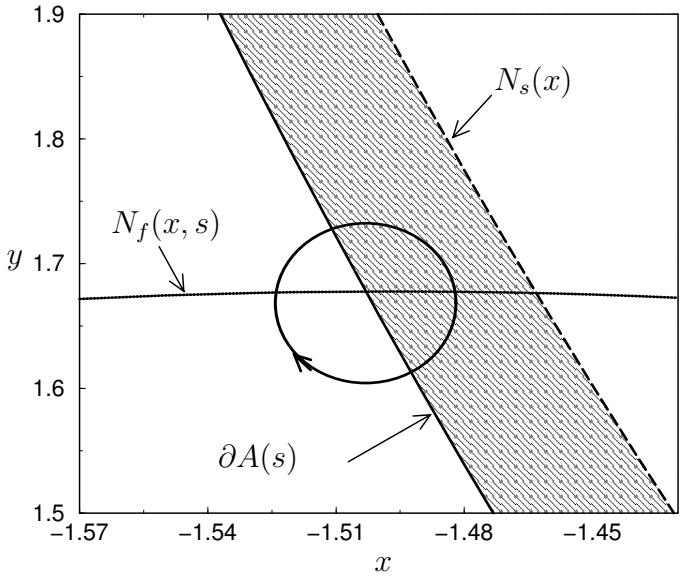

Figure 3.8.1: Representative flow around the vortex point. The shaded region is the relevant subset of $A(s)$. When the trajectory lies above the fast nullcline it is traveling from left to right in the plane. If it is to the left of the curve $\partial A(s)$ it is traveling in the positive y-direction faster than N_f and so will pass. If the solution lies to the right of the boundary curve the nullcline will catch it. The result is a spiral structure that traps solutions.

3.9 EQUATIONS OF THE MOVING VORTEX

To perform analysis on the system near the moving vortex created by the intersection of the fast nullcline and the boundary of the set $A(s)$, we simplify by making a change of variables so that the vortex structure is always centered at the origin. Denote the intersection point of $y_{\partial A(s)}(x)$ and $N_f(x,s)$ as $(\hat{x}(s), \hat{y}(s))$. Make the linear change of variables

$$z_1 = x - \hat{x}(s)$$

$$z_2 = y - \hat{y}(s)$$

to get the system

$$\frac{dz_1}{dt} = \frac{dx}{dt} - \frac{d\hat{x}}{ds}\frac{ds}{dt} \tag{3.15}$$

$$\frac{dz_2}{dt} = \frac{dy}{dt} - \frac{d\hat{y}}{ds}\frac{ds}{dt} \tag{3.16}$$

which we will write

$$\frac{dz_1}{dt} = F_1(z_1, z_2, s) \tag{3.17}$$

$$\frac{dz_2}{dt} = F_2(z_1, z_2, s) \tag{3.18}$$

where the evolution of s is governed by equation (3.7). the functions F_1 and F_2 are

$$F_1(\vec{z}, s) = -f(z_1 + \hat{x}(s)) + z_2 + \hat{y}(s) - I(s)(z_1 + \hat{x}(s)) + \frac{s}{\tau_{syn}}\frac{d\hat{x}}{ds}$$

$$F_2(\vec{z},s) = -\epsilon(z_2 + \hat{y}(s) + \frac{1}{4}(z_1 + \hat{x}(s))^5) + \frac{s}{\tau_{syn}}\frac{d\hat{y}}{ds}$$

We use the identity

$$\frac{dz_1}{dt} = \frac{dz_1}{ds}\frac{ds}{dt}$$

to write the system as

$$\frac{dz_1}{ds} = -\frac{\tau_{syn}}{s}F_1(\vec{z},s)$$
$$\frac{dz_2}{ds} = -\frac{\tau_{syn}}{s}F_2(\vec{z},s)$$

Explicit formula for $\frac{d\hat{x}}{ds}$ and $\frac{d\hat{y}}{ds}$ can be obtained, though they are too cumbersome to write here. The procedure used is to solve the equation

$$y_{\partial A(s)}(x) = N_f(x,s)$$

for $\hat{x}(s)$, and differentiate the expression with respect to s. Since $\hat{y}(s) = N_f(\hat{x},s)$ we evaluate the derivative

$$\frac{d\hat{y}}{ds} = \frac{d\hat{x}}{ds}N_f(\hat{x},s) + N_{f_s}(\hat{x},s)$$

Assume that s is fixed as a parameter. We can compute the linearization of the system (3.17)- (3.18) about the vortex point $(z_1, z_2) = (0, 0)$. It is important to note that when s is a parameter the structure at the origin is not a fixed point. However, we do expect that the eigenvalues corresponding to the linearization about the origin will give information concerning whether or not the surrounding neighborhood of the vortex is attracting, and the strength of that attraction. The change of variables used to shift the vortex structure to the origin incorporates the parameter τ_{syn} into the linearization about the vortex. It can be seen from figure 3.9.1 that the value of s that results in a stability change, or where the real part of the eigenvalues changes sign, depends on τ_{syn}. Also, equally encouraging, is that

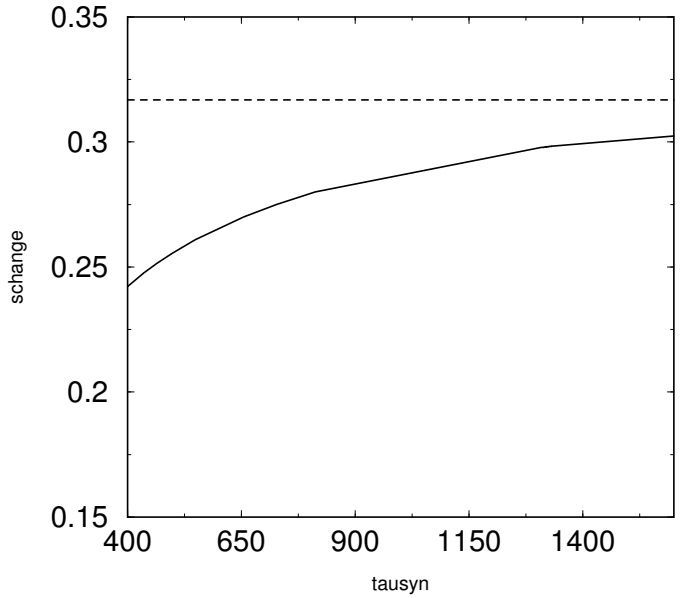

Figure 3.9.1: Value of s where the change in stability takes place. The dotted line is the value of s where the real part of the eigenvalues of the linearization about the intersection of nullclines vanishes. The solid line is where the real part of the eigenvalues corresponding to the vortex curve vanish.

this change occurs at a lower value of s than the similar occurrence at the intersection of the nullclines. The analysis performed in the previous section resulted in overestimates of the release value of s. Since the vortex structure is attracting for a longer interval of time, we expect that trajectories that are attracted will remain near longer, once the stability has changed. Both dependence on τ_{syn} and a lower value for the change of stability are apparent in simulations but are not a part of the analysis in section 3.7.

3.10 RELEASE ANALYSIS ABOUT THE VORTEX

Because the real component of the eigenvalues vanishes at a smaller value of s for the linearization about the vortex point than for the corresponding linearization about the intersection of the nullclines, we expect that using a variational equation about the vortex point will result in a superior estimate for the release value of s, at least for all but extremely large values of τ_{syn}.

The method for obtaining estimates based on the curve of vortex points is the same as that performed in section 3.7. We write the system (3.17)- (3.18) in vector form

$$\frac{d\vec{z}}{ds} = -\frac{\tau_{syn}}{s}\vec{f}(\vec{z}, s) \tag{3.19}$$

and so the equation of variation about the vortex curve $(0, 0, s)$ is

$$\frac{d\vec{z}}{ds} = -\frac{\tau_{syn}}{s}\vec{f}_{\vec{z}}(0, 0, s)\vec{z} \tag{3.20}$$

where

$$\vec{f}_{\vec{z}} = -\frac{\tau_{syn}}{s}\begin{pmatrix} -\frac{3}{4}\hat{x}(s)^2 + 2 - I(s) & 1 \\ -\epsilon\frac{5}{4}\hat{x}(s)^4 & -\epsilon \end{pmatrix} \tag{3.21}$$

Note that this is identical to the linearization in section 3.7, but centered at the vortex point rather than at the intersection of the nullclines. The solution to (3.20) can be written

$$\vec{z}(s) = \exp\left(-\tau_{syn}\int_{s_0}^{s}\frac{1}{\omega}\vec{f}_{\vec{z}}(0,0,\omega)d\omega\right)\vec{z}(s_0) \tag{3.22}$$

We use the function in (3.22) to approximate the release value of s by solving the equation

$$\|\vec{z}(s)\|_2 = \left|\left|\exp\left(-\tau_{syn}\int_{s_{enter}}^{s}\frac{1}{\omega}\vec{f}_{\vec{z}}(0,0,\omega)d\omega\right)\vec{z}(s_{enter})\right|\right|_2 \tag{3.23}$$

for s. The results are shown in figure 3.10.1. The results are quite good. The curve of approximation values follows the curve of the actual values closely for all of the values of τ_{syn} tested. In [17], under the assumption that $O\left(\frac{\epsilon}{\tau_{syn}}\right) = 1$, it is shown that the error resulting from the variational approach around the vortex point is of a smaller magnitude than the corresponding error for the curve of intersection.

The results obtained suggest that the vortex structure is the attractor for solutions during the silent phase. This implies two things. First, it offers an explicit solution to a system of ODEs during the interval of time where the synaptic variable decays. Secondly, the linearization around this curve and the corresponding variational equation closely reproduce the behavior of the full system. There is no doubt that this mechanism is responsible for the prolonged silent phase in the simple system (3.5)- (3.7). Since the foundation of the vortex structure, the set A, exists for the Hodgkin-Huxley system it is only reasonable to assume that this same mechanism is responsible for the long interspike intervals obtained via simulation. The analog to figure 3.8.1 for the HH equations is shown in figure 3.10.2.

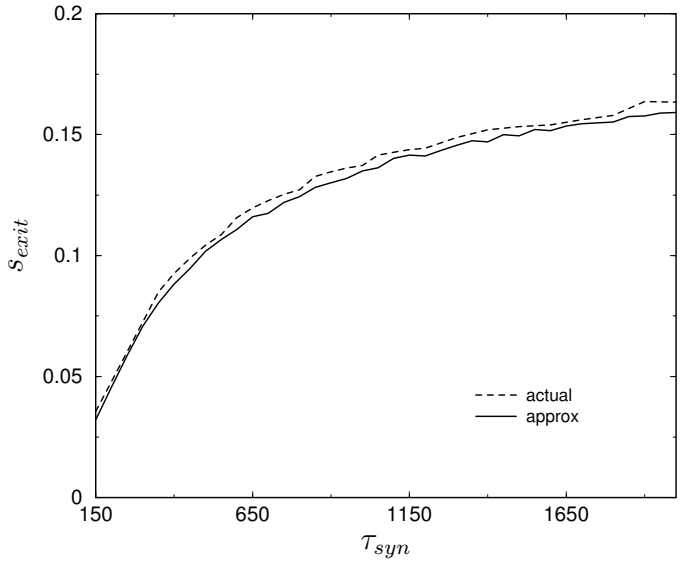

Figure 3.10.1: Comparison between the value of s_{exit} determined by the full set of equations (dotted line) and the value obtained using the variational equation. The results are quite good. For this figure $s_{enter} = 0.5$ and $\eta = 0.3$. The initial values used are $z_1 = -\eta$ and $z_2 = 0$ for both the full system (3.17)- (3.18) and the variational equation.

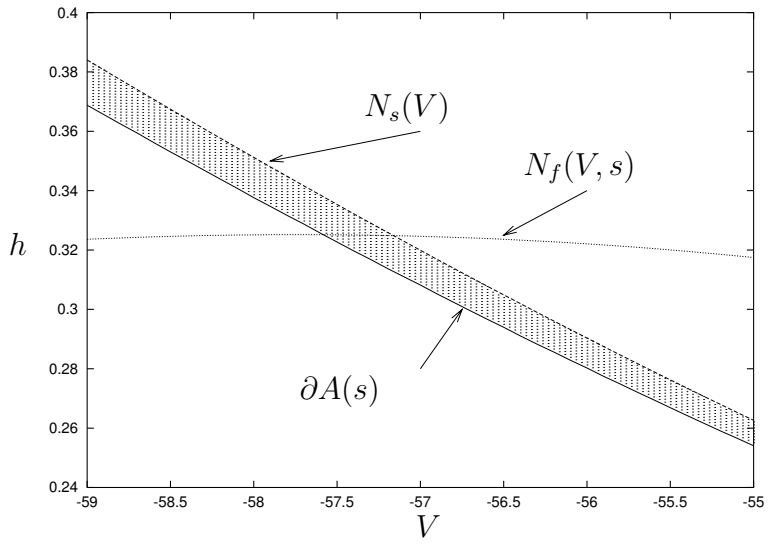

Figure 3.10.2: The relevant part of the set A for the Hodgkin-Huxley system (3.2)- (3.4) is shaded. This provides the foundation for the vortex structure to exist for this system. There is no doubt that the extremely long ISIs are the result of the behavior of solutions near this structure.

3.11 DETAILS OF THE CALCULATIONS

This section serves to describe how equations (3.12) and (3.23) are solved. The procedure is identical for each curve. The equation to be solved is

$$\left|\left|\exp\left(-\tau_{syn}\int_{s_{enter}}^{s}\frac{1}{\omega}J(\omega)d\omega\right)\vec{v}_0\right|\right|_2 = ||\vec{v}_0||_2 \tag{3.24}$$

For the system (3.5)- (3.7) the matrix $J(s)$ is the linearization matrix about the relevant point for each s. For the analysis done in section 3.7 this matrix is the linearization around the fixed point for s fixed. For the analysis discussed in section 3.10 it is the linearization around the intersection of the boundary of the trapping set and the nullcline corresponding to the fast variable. In either case, the relevant curve of points can be obtained via the quadratic formula and hence exact expressions are available.

For both curves the software *MAPLE* [51] provides a symbolic evaluation of the integral in equation (3.24). The integrated matrix has two complex conjugate eigenvalues and thus is diagonalizable. We apply the diagonalization to determine the exponential of the matrix as in [34]. The matrix-vector multiplication and the evaluation of the 2-norm were carried out using LAPACK (Linear Algebra package) and BLAS (Basic Linear Algebra Subroutines). The equation was solved using bisection [3].

3.12 τ_{SYN} LARGE

For values of τ_{syn} very large, where s evolves more slowly than h, the two methods presented here are equivalent. In the $\tau_{syn} \to \infty$ limit the curve of vortex points is identical to the curve

of points defined by the intersection of the nullclines. Figure 3.7.1 shows that the error in the approximation around the intersection is decreasing as τ_{syn} increases. The curve defined by the vortex points is a superior approximation for values of τ_{syn} where s and h evolve on similar timescales. It also provides a good approximation for large values of τ_{syn}, though it is unlikely that this mechanism would be uncovered since the more intuitive approach using the intersection of the nullclines would provide an adequate approximation.

3.13 SUMMARY

It is common that coupling excitatory cells will accelerate firing for cells that fire intrinsically [28]. In this section we have uncovered a mechanism that causes a network of Hodgkin-Huxley neurons receiving super-threshold stimulation to drastically slow down. The interspike intervals (ISIs) increase as the synaptic current decay rate decreases. In the absence of synaptic connections the system fires at a given frequency. Turning on the coupling causes the cells in the network to rapidly synchronize, with the exception of some subthreshold oscillations. The cells, thus synchronized, continue to fire since each receives a constant input that is above threshold. The synchronized network exhibits the long ISIs.

Because the network is homogeneous and rapidly synchronizes we are able to use a self-coupled model for a single cell to analyze the entire network. We deduce the important characteristics, relevant to the slow firing, from the self coupled system and construct a simple system where evolution of the variables is controlled by polynomial expressions in those variables and possesses the identified characteristics.

We use this simpler system to identify possible mechanisms that cause a prolonged silent

phase. First, we view the system as a projection on the phase plane. When parameterized by the synaptic variable the phase plane has a fixed point. When the value of the synaptic variable is above a bifurcation value, the fixed point is stable. For values of s below the bifurcation value the fixed point is unstable. Since the synaptic variable decays in time, solutions of the system should approach the intersection at first. Once the bifurcation value is reached, the intersection begins to repel solutions. We use a variational equation, or way-in way-out function, to approximate solutions in a neighborhood of this curve. The variational equation relates the strength and duration of the attraction/repulsion before and after the change in stability. The approximation obtained is not good for the case where the synaptic variable evolves on a similar time scale as the gating variable.

The second curve that we consider is a vortex structure that traps solutions in its vicinity for an extended period of time, relative to the intersection of the nullclines. This structure is the consequence of a comparison between the rates of evolution of the fast nullcline (determined by the synaptic variable) and the slow gating variable. We identify this trap in the simple model and use the same type of analysis to show that the vortex mechanism is the working attractor and that trajectories are drawn to it while the synaptic variable decays. The results of the analysis are quite good. The variation equation taken along this curve reproduces, quite accurately, the behavior of solutions during the silent phase. The way-in way-out analysis gives extremely accurate values for the exit value of s.

This trapping mechanism is a canard in three dimensions [52]. The orbit is drawn towards a curve of point that represent stable fixed points in the plane. As time increases the curve of fixed points passes through a Hopf bifurcation causing the this curve of critical points to switch from attracting to repelling. The solution remains near the unstable critical curve for

an extended period of time.

The reduced HH system (3.2)- (3.4) possesses an equivalent trapping mechanism. It is concluded that this is the mechanism responsible for the long ISIs as seen in figure 3.1.1.

In [17] it is shown how this mechanism can be applied to bursting behavior. The fixed point is unstable for small s. If s is fixed at such a value, the system will fire repeatedly since there is no change for the orbit to get drawn into the trap. If the recovery of s is sufficiently slow during the active phase the orbit will reach the left branch of the fast nullcline while the fixed point is unstable. This will result in another spike. Once the recovery of s exceeds the bifurcation value during the active phase the orbit will be drawn into the trap and the described long silent interval will take place. The number of spikes per burst depends on how quickly the synaptic variable recovers. Slower recovery will result in larger bursts. Fast recovery will result in fewer bursts. In figure 3.1.1 there is only a single oscillation since the recovery of s is sufficiently fast to allow the trap to take effect.

4.0 PHASE BOUNDARIES AS ELECTRICALLY INDUCED PHOSPHENES

The final problem that I discuss is a model for a retinal visual phenomena. As in the previous chapters, the problem involves non-local coupling of nodes in a medium. Unlike the problems presented so far, the local dynamics are not excitable and, in the case of a reduced model that we present, not oscillating. The local dynamics that we consider are bistable so that, in the absence of coupling, nodes will eventually converge to one of two steady states. The coupling that we use allows synchrony as a persistent solution so that if a node is 'ahead' of a neighbor it is held back. Similarly, if a given node is 'behind' its neighbors it catches up.

We consider two models. The first is a two-dimensional grid of integrate and fire cells developed to reproduce the visual patterns reported by subjects in an experiment to be described next. In the second part of the chapter we discuss an evolution equation that captures the major behavioral characteristics of the full model.

In experiments performed by R.H.S. Carpenter [9] subjects immersed his/her eyes in a saline bath. Alternating current is passed through the bath and the subject looks at a uniformly lit screen. When the light is interrupted to the subject's eye by a *moving* object sweeping across the visual field, parallel lines, called phosphenes, appear at the retreating edge of the object. The spacing of these lines is shown to depend only on the frequency of

the current and the velocity of the retreating edge. Carpenter shows, by varying the velocity of the moving edge and the period of the stimulus, that there is exactly one line left in the wake of the edge for every cycle of the AC stimulus. In order for the phosphenes to appear, movement of the dark edge is necessary. The apparatus for this experiment is shown in figure 4.0.1. Two methods of interrupting the visual field are used. The first is a rotating shutter with gaps so that the velocity of the retreating edge can be controlled. The other method uses an oscilloscope where a sine wave is displayed with such high frequency relative to the time base that it appears as a moving edge. The oscilloscope was useful in controlling the temporal relationship between the alternating current and the moving edge.

Carpenter cites [7] to claim that the phosphenes are not the result of any post-retinal processing, but take place in the eye itself. Accordingly, we do not assume any cortical involvement in our model. Carpenter suggests two mechanisms which may form these lines in the retina.

Carpenter first considers the possibility that the lines are interference fringes resulting from *differences in conduction times in different parts of the retina as a result of differences in the degree of illumination they receive* [9]. The author then provides evidence why this is not supported experimentally. He notes that if the illumination is increased, the gradient of conduction delays would steepen and lead to a change in the line spacing. However, the experiments show that the spacing of the lines depends exclusively on the period of the driving stimulus and the velocity of the retreating dark edge, and so this hypothesis is disregarded.

Carpenter's second hypothesis is the following: *The lines represent nodes, separating areas of the retina that are responding in antiphase to each other. The effect of a sudden*

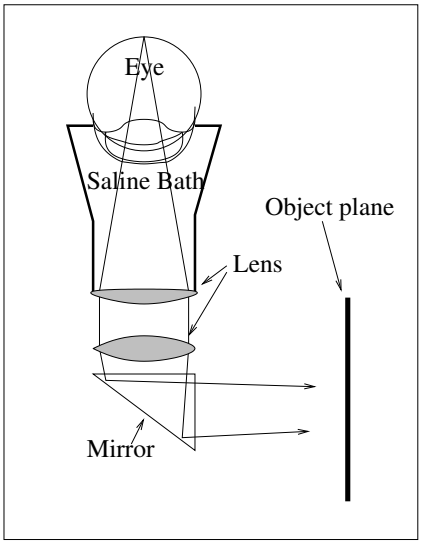

Figure 4.0.1: The experimental apparatus. The subject views a uniformly lit object plane. When the uniformly lit visual field is broken by a retreating edge the subjects report parallel lines, or phosphenes, in its wake.

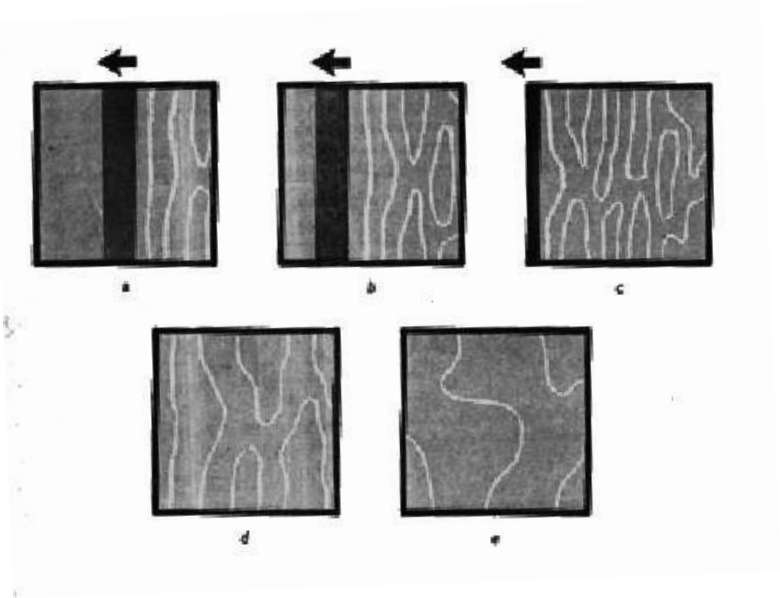

Figure 4.0.2: The lines, as reported by subjects. Immediately following the sweep of the bar parallel lines appear. As time progresses these line are perceived to move around. The lines never cross through one another, instead forming loops whenever they converge.

increase in illumination is to give an extra jolt to the system, sufficient to start a transient oscillation at the driving frequency. Assuming this hypothesis, the retina is divided into regions firing in antiphase with neighboring regions, though each is phase locked with the driving stimulus. The lines witnessed are the boundaries separating clusters firing in antiphase with one another. This is the hypothesis we explore in the present chapter.

A model of these experiments was presented by Willis in [54]. In his paper, the author used a model with two fixed points to represent regions of phase. The author considers a grid of H-cells (horizontal cells), each associated with a group of R-cells that it makes synaptic contact with. In his model it is assumed that the applied alternating current induces the following:

1. *The interaction between an R-cell (receptor cell) and the H-cell (horizontal cell) at the corresponding point is modified in such a way that the system admits two distinct limit cycles.*
2. *Interactions between R-cell groups and H-cells at neighboring points are modified by the component of applied current parallel to the retinal surface. The current can induce transitions between the limit cycles in such a way as to produce patterned shifts in the line phosphenes.*

The author uses a linear system where the R receive a tonic excitation, and the H cells receive a tonic inhibition. R and H cells communicate with each other synaptically according to the system

$$\begin{pmatrix} R' \\ H' \end{pmatrix} = \begin{pmatrix} 1 \\ -1 \end{pmatrix} + \begin{pmatrix} -\alpha & -\beta \\ \beta & -\alpha \end{pmatrix} \begin{pmatrix} R \\ H \end{pmatrix} \tag{4.1}$$

Where α and β are positive parameters. α is the strength of the negative feedback that both H and R cells are subject to. β is the strength of the interaction between an H cell and the corresponding R cell. In Willis' paper, it is assumed that the two interactions are equal and opposite, so that $\alpha = \beta$.

Now, if the effect of synaptic excitation or inhibition on H is reversed, the system becomes

$$\begin{pmatrix} R' \\ H' \end{pmatrix} = \begin{pmatrix} 1 \\ -1 \end{pmatrix} + \begin{pmatrix} -\alpha & -\beta \\ -\beta & -\alpha \end{pmatrix} \begin{pmatrix} R \\ H \end{pmatrix} \tag{4.2}$$

The system described by (4.1) has damped oscillatory solutions that converge to a fixed point. The system described by (4.2) has two stable fixed points (when constrained by the conditions $0 \leq R \leq R_{max}$ and $0 \leq H \leq H_{max}$)

In Willis' model, the boundaries are determined by the locations where the system switches states. The linear systems used are somewhat artificial since the steady state behavior is a result of domain restrictions. The model that we present is more similar to a spiking model. The machinery that we use to simulate the creation of the lines is supported by experimental results.

In this chapter, we assume that the alternating current excites a population of retinal cells. For a stimulus of appropriate strength and frequency the cells can only fire on every other cycle of the stimulus and are hence 1:2 phase locked with the stimulus. This creates a bistability. A cell in an uncoupled network could fire on either the odd or even cycles of the current. In [13], it is shown experimentally that the salamander retinal cell response to periodic pulses of light yields this phase locking. They also perform electroretinograms on humans. The authors chose to look at the physiology of the salamander retina since their

eyes are similar in structure to that of humans. The authors find that the photoreceptors are capable of 1:1 phase locking with the stimulus but that the ganglion cells follow 1:2. This suggests that the 1:2 phase locking occurs between the photoreceptors and the ganglion cells.

In our model, we suggest that the horizontal cells fire 1:2 with the stimulus. These cells are coupled with gap junctions. Because gap junctional coupling can alter the stability properties of the resting states, or phase locked states, we use biased strength of coupling to initiate the movement of the phosphenes. This is analogous to heterogeneities in the strength of interaction between retinal cells.

In the second part of this chapter we consider the following evolution equation

$$\frac{\partial u}{\partial t}(x,t) = H(u(x,t)) + c\int_{-\infty}^{\infty} w(x-y)D(u(x,t)-u(y,t))dy \tag{4.3}$$

where $u : \mathbb{R} \times (0,\infty) \to \mathbb{R}$. The function H is continuously differentiable and periodic with period $2a$. Additionally, H satisfies

$$H(0) = H(a) = 0$$

$$H'(a) = \beta < 0.$$

$$H'(0) > 0$$

The interaction function, $w(x)$, is an even and positive function that decreases as the argument gets farther from zero. We also normalize so that $\int w = 1$. The function D, like H, is periodic, with twice the period of H. In addition we require that $D'(0) < 0, D(0) = 0$ and D be continuous on the entire real line.

This equation was developed as a reduced version of the full model for the experiments. The local dynamics are bistable. For the full model, the attractors are a pair of phase locked solutions. For the reduced model the attractors are the locations where H vanishes and has a negative first derivative. The coupling, like the full model, admits uniformity as a locally stable solution.

This analysis of this equation is similar to the work in [5, 6]. We prove the existence and stability of stationary solutions that are not continuous under conditions on the parameters and the functions H and D. We describe a mechanism that results in traveling wave solutions when the stationary solutions do not exist.

4.1 THE MODEL

As described in the introduction, we model the cells responsible for the phosphenes as cells able to produce spikes when a sufficient stimulus is presented. We use an integrate and fire model where the spikes are captured by a reset, an artificial jump discontinuity in the solution. The applied current will be represented by a time dependent sinusoidal.

Carpenter's hypothesis suggests that the lines are divisions between regions that are out of phase with one another. We accomplish this by choosing a parameter regime such that each oscillator has as a solution phase locked 1:2 with the driving current. The existence of one of these phase locked solutions implies the existence of another, since the network is identical during the 'odd' and 'even' cycles. The second phase locked solution is simply a translate of the first.

In our model, an individual cell is governed by the system

$$\frac{dx}{dt} = -x - z + A\sin\left(\frac{2\pi t}{T}\right) \tag{4.4}$$

$$\frac{dz}{dt} = -\frac{z}{\tau} \tag{4.5}$$

The variables x and z are real. The parameter A is the amplitude of the driving stimulus, and T is the period. We assume that both A and T are positive. The driving stimulus is the analog to the alternating current in the experiments. The reset criterion is given by

$$x(t^-) = x_{spike} \rightarrow x(t^+) = x_{reset}; z(t^+) = z(t^-) + z_{jump}.$$

For the remainder of this section, we assume the parameter values to be $x_{spike} = \pi$, $x_{reset} = -\pi$, and $z_{jump} = 1$.

The purpose of the refractory variable, z, is to make the 1:2 phase locking robust. In the absence of the explicit refractory variable the oscillations reach near threshold during every cycle of the driving current. When a solution to an uncoupled cell is found explicitly it can be shown that the desired behavior of 1:2 locking is present. Nevertheless, we wish to use numerical methods when the network is coupled. Small numerical inaccuracies may cause undesired resets in the coupled network, where an explicit solution is not possible, and so the refractory variable is used to keep the nodes away from threshold if they should not spike on a particular cycle.

We now try to find values of the parameters that result in the desired phase locking characteristics. Explicit solutions to the system (4.4)- (4.5) are possible, however it is not known what the phase relationship is between the variable x and the driving current at the

time when the oscillator resets. To remedy this, we shift the stimulus so that we can assume that the reset criterion is met at $t = 0$. We write (4.4) as

$$\frac{dx}{dt} = -x - z + A\sin\left(\frac{2\pi(t - t_i)}{T}\right) \tag{4.6}$$

with the initial condition $x(0) = -\pi$, the reset value of x. The value of t_i is the time during a cycle of the stimulus when the system resets.

Equation (4.5) can be solved explicitly, given an initial condition. We denote this initial condition by z_0 and rewrite equation (4.6) as

$$\frac{dx}{dt} = -x - z_0 e^{-t/\tau} + A\sin\left(\frac{2\pi(t - t_i)}{T}\right) \tag{4.7}$$

The value of z_0 is easily obtained by solving the equation

$$z_0 = z_0 e^{-2T/\tau} + 1$$

Substituting this into the ODE (4.7) and solving for $x(t)$ yields the following expression

$$x(t) = e^{-t}\left(-\frac{z_0 e^{t-t/\tau}}{1 - 1/\tau} + Ae^{t}\left(-\frac{\omega\cos(\omega(t + t_i))}{1 + \omega^2} + \frac{\sin(\omega(t + t_i))}{1 + \omega^2}\right)\right) + Ce^{-t} \tag{4.8}$$

where $\omega = \frac{2\pi}{T}$. C is determined by the initial condition $x(0) = -\pi$. We wish to find parameter values such that $x(t) < \pi$ for $t < 2T$ and $x(2T) = \pi$. To find the value of t_i that satisfies the phase locking conditions, we construct a map

$$t_{in+1} = t_{in} + f(t_{in}, z_{0n}) mod(T) \tag{4.9}$$

$$z_{0n+1} = z_{0n}\exp\left(-\frac{f(t_{in}, z_{0n})}{\tau}\right) + 1 \tag{4.10}$$

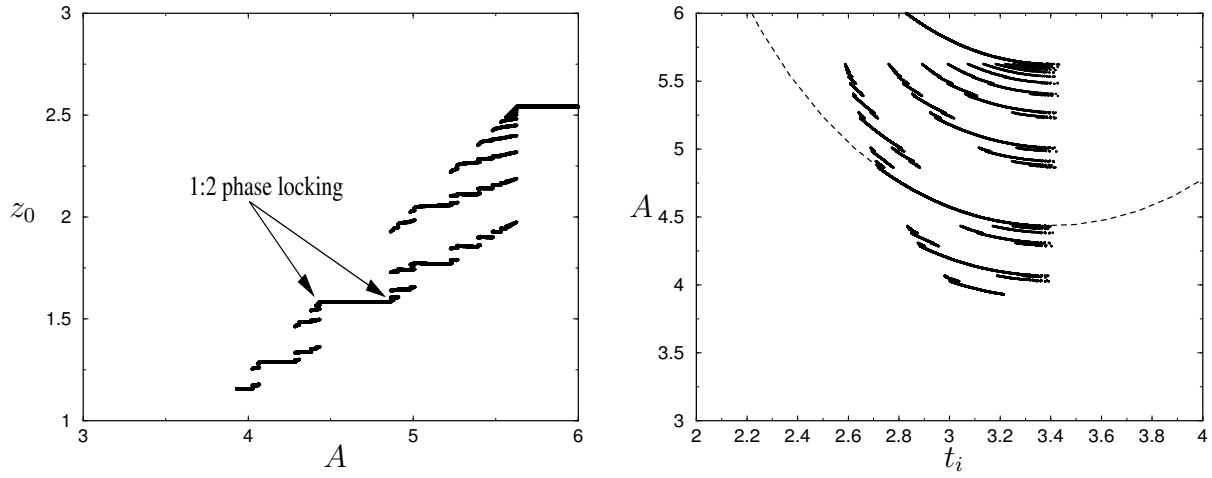

Figure 4.1.1: Left Panel: Bifurcation diagram for the map (4.9)- (4.10) as A varies. The parameter values used in this map are $T = 10$ and $\tau = 20$. The marked region is the region where the refractory variable resets to the value corresponding to 1:2 phase locking. Right panel: The limit set diagram for the values of t_i. The values of t_i corresponding to phase locked solutions are given by the intersection of the dark line and the dotted line.

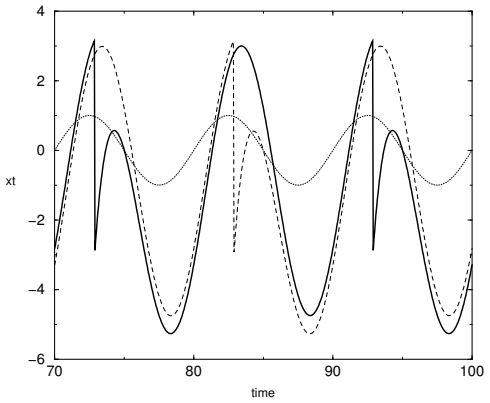

Figure 4.1.2: The phase locked solutions. Parameter values are $T = 10$, $\tau = 20$, and $A = 4.5$. The stimulus is also shown, scaled to fit. There are two phase locked solutions, the second a tranlate of the first.

The function f is the time of the next reset. The value of this function is obtained by solving equation (4.8) for the first value of t where $x(t) = \pi$. Figure 4.1.1 is a bifurcation diagram that shows the limit sets of the map defined by (4.9) and (4.10). From the figure, one can see that there is an interval in A such that the system resets once for every two cycles of the driving stimulus. Figure 4.1.2 shows a pair of phase locked solutions, each a translate of the other.

For the remainder of this section we will assume that the parameter values lie in the 1:2 phase locked regime. The pair of phase locked solutions create bistability for each cell. Given an initial condition, the corresponding solutions will converge to one of these. The basin of attraction for each of the solutions will have the same measure, since they are translations of one another.

According to Carpenter's hypothesis, it is possible that the phosphenes correspond to

the boundaries separating regions firing out of phase with one another. These regions are formed by the passing of a light blocking object. We will model the moving edge as a brief inhibition that passes over the grid.

4.1.1 Creating the Boundaries

We model the mechanism responsible for the line creation using a traveling inhibitory term. We write this as

$$bar(i,t) = \begin{cases} -d & \text{if} \quad i/v + T_0 < t < i/v + T_0 + W \\ 0 & \text{otherwise} \end{cases} \tag{4.11}$$

The index i is the node. The parameter T_0 is the time when the bar begins the pass through the visual field. W is the amount of time each node is inhibited and v is the velocity of the moving edge. The parameter d is the strength of the inhibition. The evolution of a single node is given by

$$\frac{dx_i}{dt} = -x_i - z_i + A\sin\left(\frac{2\pi t}{T}\right) + bar(i,t) \tag{4.12}$$

$$\frac{dz_i}{dt} = -\frac{z_i}{\tau} \tag{4.13}$$

In order to obtain results similar to those reported by subjects in the experiments, the value of W must be sufficiently large. The action of the inhibition is to cause certain oscillators to leave the basin of attraction of the pre-sweep solution and enter the basin corresponding to the other attractor. The passage through threshold is not immediate, and so there is a minimum amount of time that the oscillator is exposed to the inhibition that

would enable it to switch phases. In addition, Carpenters subjects reported that the lines are evenly spaced. This suggests that the amount of time that each node is exposed to the inhibition must be sufficiently long to negate any pre-inhibitory behavior. The behavior of each node after the inhibition has passed will be a function of the time when the inhibition is removed. Since the difference of time between the introduction of the inhibition and its removal is constant, we can plot the switching behavior of a node as a function of the time during the stimulus when the inhibition is first introduced. Figure 4.1.3 shows this plot.

We now consider a line of oscillators where each node is governed by equations (4.12)-(4.13). Figure 4.1.4 shows the behavior of the uncoupled network as the bar sweeps. This figure verifies that for each cycle of the driving stimulus there is exactly one boundary separating regions that reset out of phase with one another.

We have shown that our integrate and fire model can produce the boundary creation results obtained by Carpenter experimentally. For a sufficiently long inhibition we obtain equally spaced lines and the spacing has the correct dependence on both the stimulus period and the velocity of the sweep. Now, we couple the oscillators together to obtain the two dimensional images and movement reported by Carpenter's subjects.

4.1.2 Movement of the Phosphenes

Perhaps the most interesting finding in Carpenter's experiments is the movement of the phosphenes. The movement appears random, but there is some structure in how they move as a whole. There are three 'rules' that the phosphenes appear to obey:

1. Neighboring phosphenes show a tendency to move in a similar manner. That is, if a given line is bulging to the right, then it is likely that a neighboring line will bulge in the

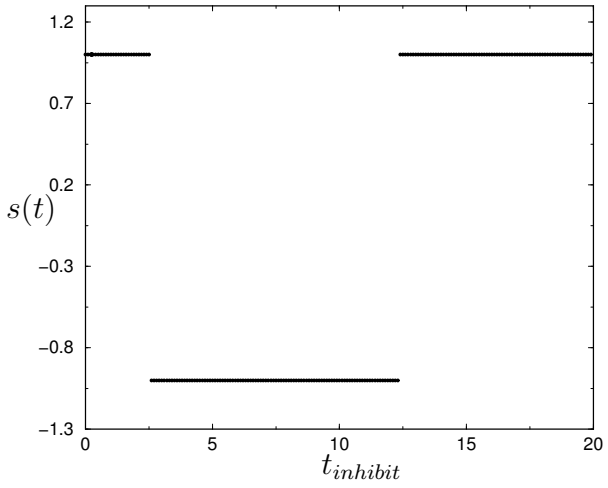

Figure 4.1.3: The binary function $s(t)$. The horizontal axis is the time during a period of an oscillation of x when the inhibition is introduced. For concreteness, $t_{inhibit} = 0$ corresponds to the time when the stimulus is zero and increasing. For this figure, $T = 10$ and because we are in the 1:2 phase locking regime we plot over two periods of the stimulus. The vertical axis is the value of a binary function $s(t_{inhibit})$. $s(t_{inhibit}) = 1$ when phase of the oscillator is the same after the inhibition as it was previous. When $s(t_{inhibit}) = -1$, the oscillator has exited the basin of attraction corresponding to the original oscillation and was attracted to the shifted, second oscillation. The values in this plot are for $W = 30$.

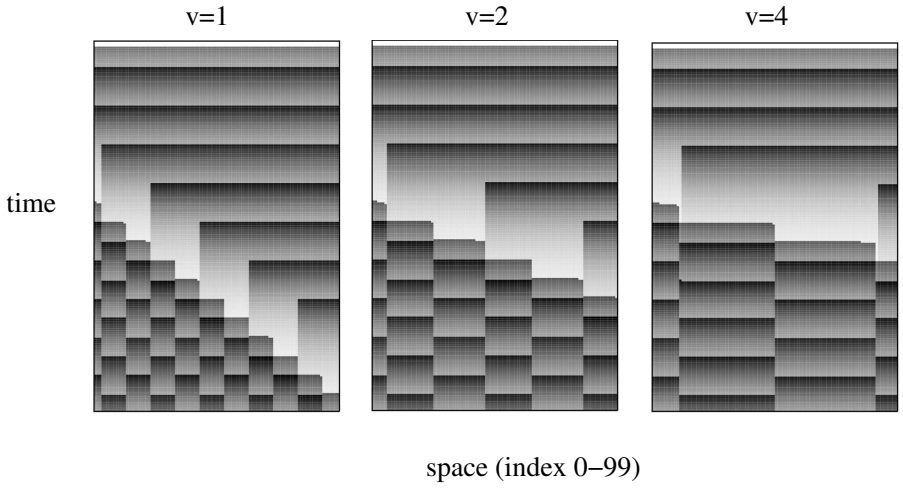

Figure 4.1.4: Three simulations of a line of oscillators inhibited by a sweep of the *bar* function. In each panel the horizontal axis is the spatial index, and the vertical axis is time, increasing from top to bottom. The velocity of the sweep is above each panel and measures the speed of the movement of the bar in index units per time. In Carpenter's experiments, one line was seen for every cycle of the stimulus. In this figure $T = 10$. For $v = 1$ there are ten cycles of the stimulus, and should be 10 lines. Similarly, for $v = 2$ and $v = 4$ there should be 5 and 2-3 respectively. These simulations confirm that our model behaves appropriately. In all three panels $W = 30$ and $d = 2$.

same direction. By no means is this an unbreakable rule, lines do occasionally collide with one another, but it is a noted behavior in the experiments

2. The lines never cross through one another. Instead, they combine to form loops.
3. A line never breaks apart unless it meets another line.

A visual description of the second item is shown as figure 4.1.5, and a prohibited scenario is depicted in figure 4.1.6. As will be seen, localized synchrony is a stable solution. In other words, when a node is on the interior of a region of oscillators firing in synchrony there is no possibility that this node will spontaneously assume the opposite phase. Only nodes on the boundary are capable of switching phases. For this reason, the second and third items above are already incorporated into this model.

Our movement mechanism is relatively simple. Suppose there are two regions, region A and region B, which neighbor each other and contain only oscillators in phase with the others in the regions. Consider the group of oscillators right on the boundary. If some of the oscillators in region B were to synchronize with those in region A, the line would move, because the newly synchronized clusters are now in region A, and so the boundary has moved. Similarly, the line could move the other way if some of the oscillators in region A synchronize with their neighbors in region B. Furthermore, if some of the oscillators in region A synchronize with those in region B, and some of those in B synchronize with those in A, the line moves in one direction in some spatial locations, and in another direction at another location. Figure 4.1.7 shows the transition of a line.

4.1.2.1 The Coupling Terms The coupling has to have a number of characteristics, inspired by the movement 'rules' stated in the previous subsection. The second and third

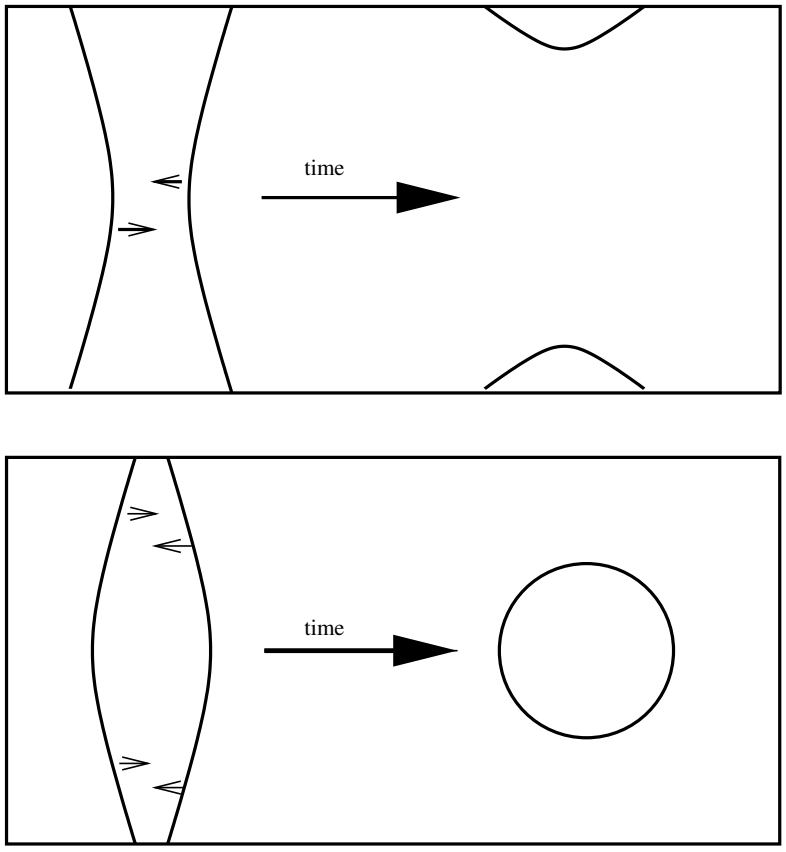

Figure 4.1.5: Meeting of the phosphenes. The lines do not cross one another, but instead annihilate one another, forming new patterns such as loops.

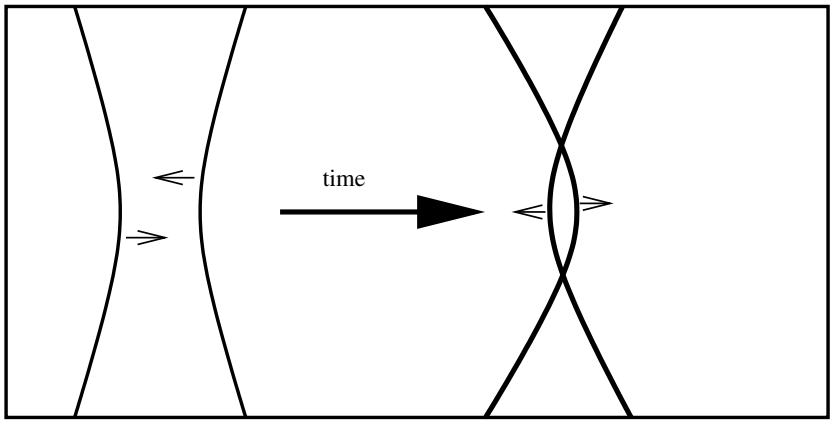

Figure 4.1.6: The lines cross, but remain intact after the collision. This scenario is not possible.

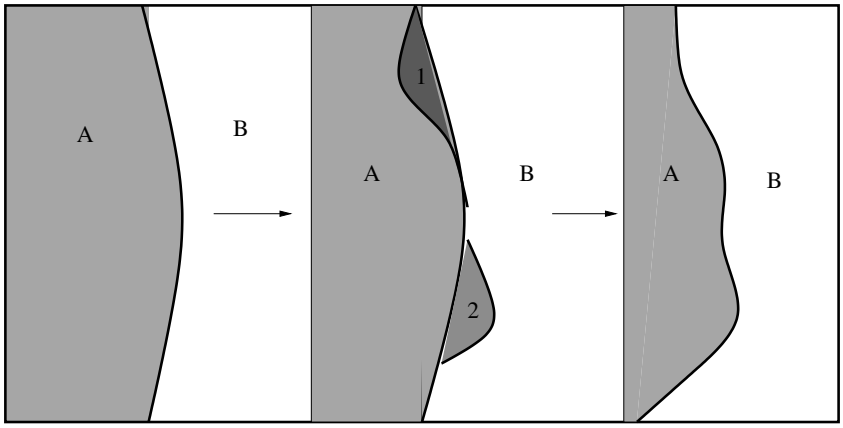

Figure 4.1.7: The movement of a phosphene. The leftmost panel shows the regions A and B initially. The middle panel shows regions, 1 and 2, that are about to switch phase by synchronizing with regions B and A respectively. The resulting line is shown in the right of the figure. The arrows indicate passage of time.

item make it essential that the coupling cause synchrony to be a locally stable solution. Also, because we are dealing with the *phase* of an oscillator, we would like the coupling to be periodic with period 2π. The coupling we chose has the form

$$cf_d \sin(x_d - x_{i,j}) \tag{4.14}$$

where $d = \{up, down, left, right\}$ (eg. $f_{up} = f_{i,j-1}$). The coefficients f_d are positive and discussed in detail in the next subsection. In this chapter we restrict ourselves to the case of nearest neighbor coupling. The parameter c is always positive and determines the linear strength of the coupling, and is the same for each node. The evolution of the nodes in the coupled network is governed by the equation

$$\frac{dx_{i,j}}{dt} = F(x_{i,j}) + c\sum_d f_d \sin(x_d - x_{i,j}) \tag{4.15}$$

4.1.2.2 The Coupling Coefficients f_d The first rule of movement stated previously was not a hard-and-fast rule, but more of an observed trend. Before we can describe how we incorporate this rule into the simulation, we need to explain the basic mechanism of movement we have chosen.

Suppose we have one oscillator, A, with four neighbors, N_j, $j = 1, .., 4$ (figure 4.1.8). Suppose that N_1 and N_2 are firing synchronously (with one another), and N_3 and N_4 are firing at the other phase. The phase that A synchronizes to depends on the relative strengths of the coupling. For example, suppose that $f_{up} + f_{left} >> f_{right} + f_{down}$. Then, oscillator A will synchronize with N_1 and N_2. If the relative difference between coupling strengths is not so high, there will be an intermediate phase for A, which will in turn alter other nearby oscillators. Eventually, oscillator A will be on the interior of a region and will synchronize

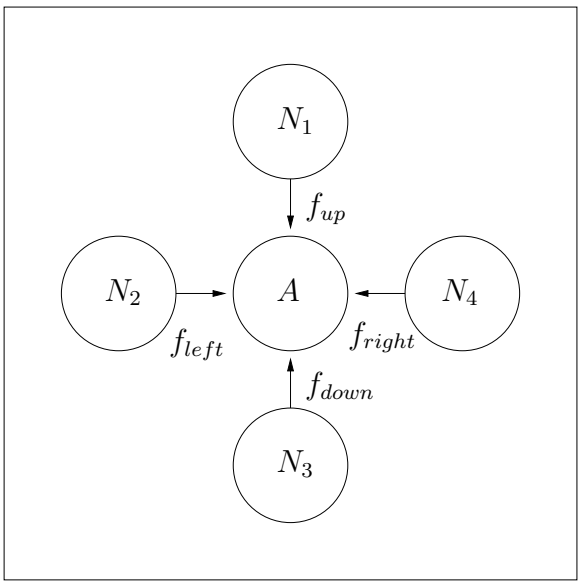

Figure 4.1.8: coupling diagram

with the others there. The phosphenes are represented by the boundary of the regions of in phase oscillators, where they temporarily assume a parameter dependent (relative sizes of f_d), and neighbor dependent, phase until they are enveloped into the interior of a region. Once this process is complete, the line (boundary) will have moved.

Because the direction of the movement depends on the relative coupling strengths, we wish to structure the coefficients, f_d, spatially. Suppose we have a single line of oscillators. If, for every oscillator, $f_{right} > f_{left}$ we expect each to synchronize with its neighbor to the right, thus moving the lines left. Thus, to implement the first item from early in this section (nearby lines have a tendency to move in the same direction) we define regions of monotonicity. Thus, there will be spacial intervals where $f_{left} > f_{right}$ and others where $f_{right} > f_{left}$. Two lines in the same region of monotonicity will move in similar directions.

This is the spacial structure of f. A difficulty is that it is not clear how many 'flat spots' there should be in f. In other words, how many times in the domain should the sign of $f_{right} - f_{left}$ change? When simulating, we changed the monotonicity at most 3 times in both the vertical and horizontal directions. The implementation used in the simulation code is described in the next section.

4.1.3 Simulation

Simulations were done using Runge-Kutta fourth order integrator, with a constant time step. The reset is accomplished by setting $x_{i,j}(t_k) = -\pi$ and $z_{i,j}(t_k) = z_{i,j}(t_k) + 1$ whenever $x_{i,j}(t_k) > \pi$. No interpolation is done, so the resets will always occur at a multiple of the time step. The time step used is $\Delta t = 0.01$.

All simulations are done on a 100x50 oscillator grid. The coupling strength array, $f_{i,j}$ was determined as follows:

1. Choose, randomly, 3 indices in the horizontal domain (h_1, h_2, h_3), and 3 more in the vertical domain (v_1, v_2, v_3). Assume that $h_1 < h_2 < h_3$ and $v_1 < v_2 < v_3$. The choice of 3 set indices is motivated by figures in [9]. This implementation can be extended to incorporate any number of set nodes, up to the number of nodes present in the grid.
2. Define two arrays, H and V, (for horizontal and vertical) with the appropriate number of elements. For our purposes H has 100 elements (the width of the grid) and V has 50 elements (the height of the grid).
3. Assign to the array elements $H(1)$, $H(h_1)$, $H(h_2)$, $H(h_3)$ and $H(100)$ random values between 0 and 1.
4. The grid is now divided into rectangles. Divide each of these rectangles into two right

triangles. In the simulations presented here, the diagonal goes from the top left to the lower right.

5. Using the three corners of the triangles, compute the value at the indices inside each triangle according to the plane the corner values define (see figure .

This will produce the array f with regions of monotonicity.

Simulations were carried out using some FORTRAN code, using calls to LAPACK and BLAS to do the vector operations in the RK integrator. The graphical output was produced using the PGPlot package.

Figure 4.1.10 shows output from a sample run of the simulation.

4.2 A REDUCED MODEL

In this section we consider a reduced model analogous to the full model presented in the first part of this chapter. This model captures two important aspects of the full model. First, the model is intrinsically bistable. The uncoupled system will converge, pointwise, to one of two solutions depending on which basin of attraction the initial conditions lie in. Secondly, sufficiently strong coupling will cause the network to assume a uniform profile. This is analogous to synchrony in the full model.

The equation that we consider is

$$\frac{\partial u(x,t)}{\partial t} = H(u(x,t)) + c\int_{-\infty}^{\infty} J(x-y)D(u(x,t)-u(y,t))dy \tag{4.16}$$

where H satisfies

$$H(-1) = H(0) = 0$$

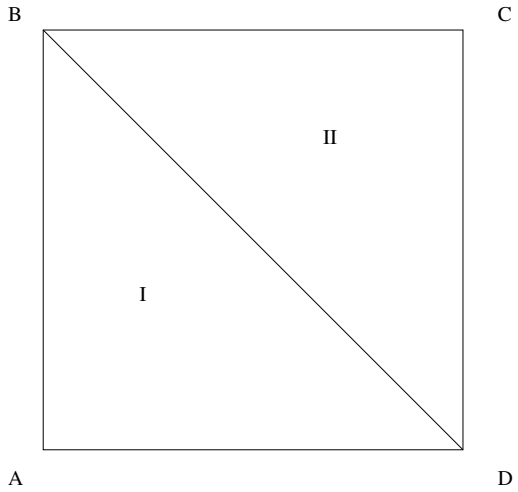

Figure 4.1.9: A diagram that shows how the biased coupling is determined for the simulations. The value of the function is chosen randomly at the vertices A,B,C,D. The rectangle is divided into two triangles. The value of the coupling function for points in these triangles is determined using a linear interpolation of the three vertices that form the triangle. For example, if a node lies in the region marked II, the value of the relative coupling strength at that node is determined by the plane that crosses the determined points at B,C, and D.

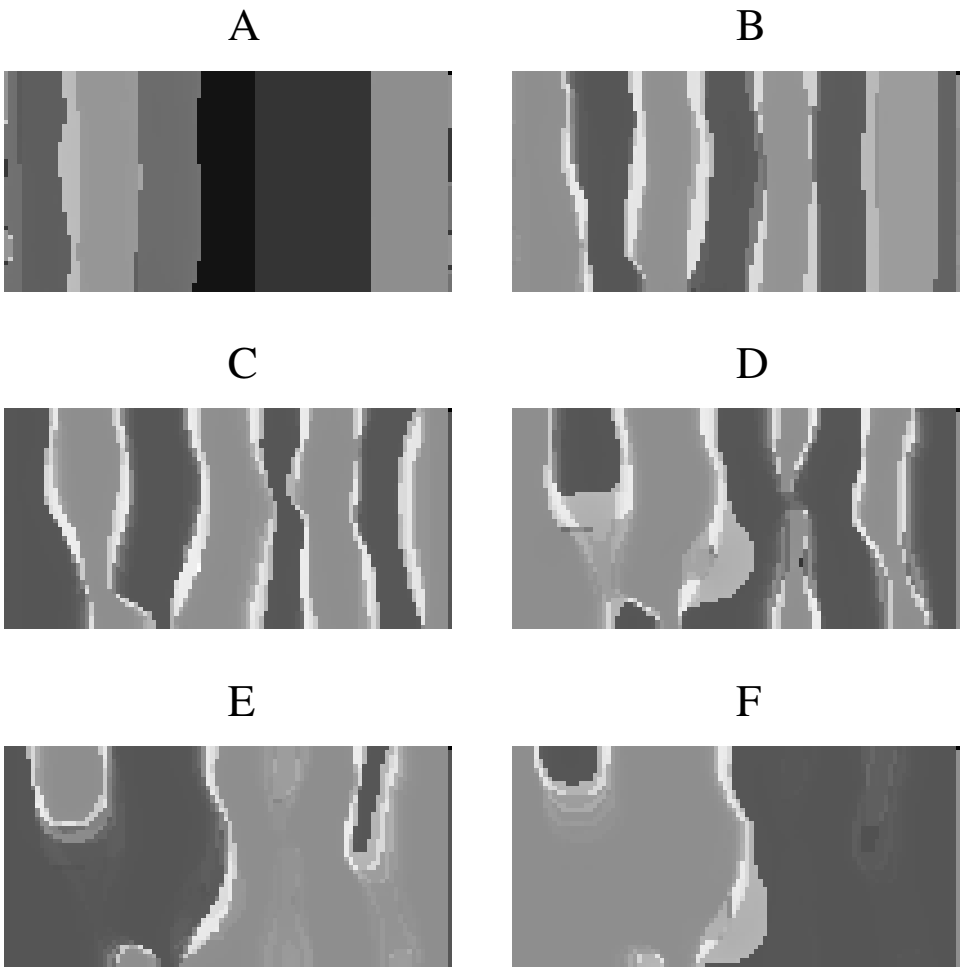

Figure 4.1.10: Simulation of the integrate and fire model on a 100x50 oscillator grid. Each panel shows the field after a set increment of time. The variable plotted is z, the refractory variable. In panel A, the bar is about to complete the pass. Lines (or regions) have formed on the left edge and have begun to move. In panels B,C, the lines are clearly defined and moving. In panel D, synchronous regions 'poke holes' through a region in antiphase, forming two loops. Panels E F show two of the loops annihilating themselves as the region that defines them collapses. Parameter values (for equation (4.15)) are $v = 1.3$, $A = 4.7$, $T = 10$, $\tau = 20$, $d = -2$, $W = 30$, $c = 7$.

$$H'(-1) < 0$$

$$H'(0) > 0$$

Also, H is continuously differentiable and periodic with period 2. The choice of 2 is for simplicity, and one can obtain identical results for any value of the period of H. The function D is periodic with period 4 (twice the period if H for the general case) and satisfies

$$D(0) = 0$$

$$D'(0) < 0$$

In addition, we require that D be continuously differentiable so that it satisfies a lipshitz condition on the entire real line. The parameter c is real and positive. The interaction function J satisfies

$$J > 0$$

$$\int_{\mathbb{R}} J(x)dx = 1$$

$$J(x) = J(-x)$$

In [5], the authors prove the existence and stability of stationary solutions to

$$u_t = -u - \lambda f(u) + J * u \tag{4.17}$$

where $\lambda > 0$ and the function f is bistable. The authors prove that, under conditions on the parameters, there exist stable steady state solutions that are discontinuous. In this chapter we prove the existence of similar solutions to equation (4.16).

We first address the initial value problem. Suppose we have an initial condition $u(x,0)$, defined for all $x \in \mathbb{R}$. Since D is continuous and periodic it is bounded, and so the integral

$$\int_{\mathbb{R}} J(x-y)D(u(x,t)-u(y,t))dy$$

is defined for any $x \in \mathbb{R}$ and is bounded by $\pm||D||_\infty$, due to the normalization of J. Similarly, the function H is bounded so that the absolute value of the right side of (4.16) is bounded by

$$||H||_\infty + ||D||_\infty$$

For any $x \in \mathbb{R}$ we have that

$$\left|\frac{\partial u}{\partial t}\right| \leq ||H||_\infty + ||D||_\infty$$

and so the solution will not blow up in finite time for any $x \in \mathbb{R}$.

In addition, since the right side of (4.16) is defined whenever u is defined, the resulting solution $u(x,t)$ will be a continuous function in t.

It is not necessary for $u(x,t)$ to be a continuous function in x for a given initial condition. A simple example to reveal this is the case $c = 0$. Let $u(x,0)$ be a continuous function in x, which attains both positive and negative values (crosses the $u = 0$ axis non-tangentially at least once). For values of x where $u(x,0) > 0$ the solution $u(x,t)$ will converge to 1 (or $2n+1$ for $n \in \mathbb{Z}^+$). For x where $u(x,0) < 0$, the solution will converge to a steady state where $u(x,t) < 0$. Locations where $u(x,0) = 0$ are invariant. The result is a solution that is discontinuous in the variable x. We now state and prove two theorems (existence and stability) regarding these discontinuous solutions for the case $c > 0$. .

We begin with the following existence theorem:

Theorem 2 *Existence of discontinuous stationary solutions*

Suppose that the function H satisfies

- *H is an odd function with period 2.*
- *H is continuously differentiable.*
- *$H(1) = 0$ and $H'(1) < 0$.*
- *$H(0) = 0$ and $H'(0) > 0$.*

and that the function D satisfies

- *D is continuously differentiable.*
- *$D(0) = 0$ and $D'(0) < 0$.*
- *D is periodic with period 4 (twice the period of H).*

Let $\beta > 0$ be a number such that $H'(u) < 0$ for $u \in (1-\beta, 1+\beta)$ and set $\delta = -\max_{u\in(1-\beta,1+\beta)} H'(u) > 0$. Set $K = \max_{u\in\mathbb{R}} |D'(u)|$.

Choose a measurable set M and denote the complement as M^c. Assume that c is small enough so that the following conditions hold:

$$\begin{aligned} H(1+\beta) + c\overline{D}_{MM^c} \sup_{x\in M} \textstyle\int_{M^c} J(x-y)dy \le 0 \\ H(1-\beta) + c\underline{D}_{MM^c} \sup_{x\in M} \textstyle\int_{M^c} J(x-y)dy \ge 0 \\ H(-1+\beta) + c\overline{D}_{MM^c} \sup_{x\in M^c} \textstyle\int_{M} J(x-y)dy \le 0 \\ H(-1-\beta) + c\underline{D}_{MM^c} \sup_{x\in M^c} \textstyle\int_{M} J(x-y)dy \ge 0 \end{aligned} \tag{4.18}$$

where

$$\overline{D}_{MM^c} = \max_{s\in(2-2\beta,2+2\beta)} D(s)$$

$$\underline{D}_{MM^c} = \min_{s\in(2-2\beta,2+2\beta)} D(s)$$

If $-\delta + 2cK < 0$ there exists a solution, $U(x)$, satisfying

$$0 = H(U(x)) + c\int_{\mathbb{R}} J(x-y)D(U(x)-U(y))dy \tag{4.19}$$

such that

$$\begin{aligned} U(x) &\in (1-\beta, 1+\beta) \text{ when } x \in M \\ U(x) &\in (-1-\beta, -1+\beta) \text{ when } x \in M^c \end{aligned} \tag{4.20}$$

Proof:

Let

$$B = \left\{ U(x) \;\middle|\; \begin{array}{rl} U(x) \in (1-\beta, 1+\beta) & \text{when} \quad x \in M \\ U(x) \in (-1-\beta, -1+\beta) & \text{when} \quad x \in M^c \end{array} \right\}$$

and define the map

$$TU(x) = U(x) + \epsilon\left[H(U(x)) + c\int_{\mathbb{R}} J(x-y)D(U(x)-U(y))dy\right] \tag{4.21}$$

For ϵ sufficiently small, the conditions (4.18) guarantee that $T : B \to B$. Our method of proof is to show that T is a contraction mapping. This allows us to conclude that there is a solution of the type (4.20) that satisfies (4.19).

To simplify expressions, define the function

$$A(U,x) = \int_{\mathbb{R}} J(x-y)D(U(x)-U(y))dy$$

Let $U, V \in B$. We write

$$\|TU - TV\|_\infty = \|U - V + \epsilon(H(U) - H(V) + A(U,x) - A(V,x)\|_\infty$$

The quantity $A(U,x) - A(V,x)$ can be written

$$\int_{\mathbb{R}} J(x-y)[D(U(x)-U(y)) - D(V(x)-V(y))]dy$$

Because D is continuously differentiable and K is a finite number, we have that

$$|D(g-h)| < K|g-h|$$

for $g, h \in \mathbb{R}$. We have the inequality

$$\begin{aligned}
\|A(U,x) - A(V,x)\|_\infty &\leq \|cK \int_{\mathbb{R}} J(x-y)(U(x) - U(y) - V(x) + V(y))dy\|_\infty \\
&= \|cK(U(x) - V(x)) \int_{\mathbb{R}} J(x-y) - cK \int_{\mathbb{R}} J(x-y)(U(y) - V(y))dy\|_\infty \\
&\leq cK \int_{\mathbb{R}} J(x-y)dy \|U(x) - V(x)\|_\infty + cK \int_{\mathbb{R}} J(x-y)dy \|U(x) - V(x)\|_\infty \\
&= \left(2cK \int_{\mathbb{R}} J(x-y)dy\right) \|U(x) - V(x)\|_\infty
\end{aligned}$$

We may write

$$\|TU - TV\| \leq \|U(x) - V(x) + \epsilon(H(U(x)) - H(V(x)))\| + 2\epsilon cK\|U(x) - V(x)\| \tag{4.22}$$

Since $H'(U) > -\delta$ for $u \in (1-\beta, 1+\beta)$ we have that

$$H(U(x)) - H(V(x)) \leq -\delta(U(x) - V(x)) \leq 0$$

for x such that $U(x) > V(x)$ and

$$0 \leq H(U(x)) - H(V(x)) \leq -\delta(U(x) - V(x))$$

for x such that $U(x) < V(x)$. Since the value of $H(U(x)) - H(V(x))$ has the opposite sign as $U(x) - V(x)$ it follows that

$$\|U(x) - V(x) + \epsilon(H(U(x)) - H(V(x)))\|_\infty \leq \|U(x) - V(x) - \epsilon\delta(U(x) - V(x))\|_\infty \tag{4.23}$$

We may re choose ϵ small enough so that $\epsilon\delta < 1$. Substituting (4.23) into the right side of (4.22) gives

$$\|TU - TV\|_\infty \leq (1 - \epsilon\delta)\|U(x) - V(x)\|_\infty + 2\epsilon cK\|U(x) - V(x)\|_\infty$$

$$\|TU - TV\|_\infty \leq (1 - \epsilon(\delta - 2cK))\|U(x) - V(x)\|_\infty$$

and so if $\delta > 2cK$ then T is a contraction mapping and hence there is a steady state solution to (4.16).

The quantity $\delta - 2cK$ is just a comparison of the attraction to the fixed points of the intrinsic system and the strength of the coupling which synchronizes the network. If the fixed point 'wins' then the solution will not leave the β neighborhood of 1, where $H = 0$. Similarly, if the coupling overwhelms the attraction to the fixed point then the solutions will leave the β bands as they approach a more uniform profile.

We can now state the following theorem:

Theorem 3 *Linear Stability*

Assume that for a set M, a number β and a parameter c the conditions in Theorem 2 are satisfied. The resulting stationary solution is linearly stable.

Proof: Let U be the steady state solution of (4.16) shown to exist. Let $u(x,t) = U(x) + w(x,t)$. The function $w(x,t)$ satisfies the following

- $w(x,0)$ is bounded and small for every $x \in \mathbb{R}$. It is a perturbation to the steady state solution $U(x)$ for each x.
- $\int J(x-y)w(y)dy$ exists and is finite for any $x \in \mathbb{R}$.

Substituting $u(x,t) = U(x) + w(x,t)$ into (4.16) gives

$$w(x,t)_t = H(U(x) + w(x,t)) + c\int_{\mathbb{R}} J(x-y)D(U(x) + w(x,t) - U(y) - w(y,t))dy$$

We expand the right side about $U(x)$ and separate terms that are linear in w to obtain

$$\begin{aligned} w(x,t)_t = \quad & H(U(x)) + w(x,t)H'(U(x)) \\ & +c\textstyle\int_{\mathbb{R}} J(x-y)[D(U(x)-U(y)) + (w(x,t)-w(y,t))D'(U(x)-U(y))dy + O(w(x,t)^2) \end{aligned}$$

We are concerned with the linear stability and will omit the higher order terms in w. We may rewrite the equation as

$$\begin{aligned} w(x,t)_t = \quad & w(x,t)H'(U(x)) \\ & +c\textstyle\int_{\mathbb{R}} J(x-y)(w(x,t)-w(y,t))D'(U(x)-U(y))dy \end{aligned}$$

$$\begin{aligned} w(x,t)_t = \quad & w(x,t)H'(U(x)) + c\textstyle\int_{\mathbb{R}} J(x-y)w(x,t)D'(U(x)-U(y))dy \\ & -c\textstyle\int_{\mathbb{R}} J(x-y)w(y,t)D'(U(x)-U(y))dy \end{aligned} \tag{4.24}$$

Now consider how the maximum of w evolves. We know that $w(x,0)$ is bounded. We show that under the existence conditions if $w(x,t)$ is bounded for any $t \geq 0$ then $w(x,t)$ will remain bounded and decay to zero for each $x \in \mathbb{R}$. We have the following inequality:

$$\left| c\int_{\mathbb{R}} J(x-y)w(y)D'(U(y)-U(x))dy \right| \leq cK||w(x,t)||_\infty$$

This implies that

$$\frac{d}{dt}\|w(x,t)\|_\infty \leq (-\delta + cK)\,\|w(x,t)\|_\infty + cK\|w(x,t)\|_\infty$$

$$\frac{d}{dt}\|w(x,t)\|_\infty \leq (-\delta + 2cK)\,\|w(x,t)\|_\infty$$

Since $-\delta + 2cK < 0$ (Theorem 2), we have that $w \to 0$ pointwise since the maximum of w decays to zero. Hence, sufficiently small perturbations to the steady state solution will decrease to zero. It follows that the steady state solution proved to exist is also stable (linearly).

It is important to realize that the theorems 2 and 3 provide sufficient conditions for stable stationary solutions, but they are by no means necessary conditions. The approximations used in the proof can be somewhat loose, and solutions of the type that we are looking for can exist and be stable when the conditions on parameters and function H and D are not satisfied.

Notice that the only restrictions on J for the existence of these solutions is the normalization and that $J > 0$. Suppose that the parameters are such that there are no solutions of the type guaranteed by theorem. We suspect that this will cause the network to synchronize. Uniform solutions will not remain near $u = 0$ since this is unstable for the uncoupled system. If the tendency towards synchrony is great enough the long term behavior of the network on the entire real line will be a synchronous solution at one of the stable steady states, $u(x) = \pm 1$. This results in front solutions to (4.16).

The only requirements on the function D are $D(0) = 0$ and $D'(0) < 0$, and so this function can determine the direction of propagation, and will if the interaction function J is even. Similar to the directional bias used in the full model, a shift in the interaction function results in biased coupling. We hypothesis that if this shift is sufficiently large the direction of propagation will depend on which direction the interaction function is shifted. The amount that J needs to be shifted to determine the direction of propagation depends on the shape of the graph of D.

We present an example of application of theorems 2 and 3. We consider the system where $D(u) = -\sin\left(\frac{\pi u}{2}\right)$ and $H(u) = \sin(\pi u)$. The existence of stationary solutions is trivial since

$$U(x) = \begin{cases} 1 & \text{when} \quad x \in M \\ -1 & \text{when} \quad x \in M^c \end{cases} \tag{4.25}$$

is always a solution since $D(\pm 2) = 0$. For this case $\beta = 0$, $\delta = -\pi$, and $K = -\frac{\pi}{2}$. The conditions (4.18) are satisfied trivially. Theorem 3 guarantees the stability of the solution (4.25) whenever $c < 1$. As previously noted, this is a sufficient condition for stability, but not necessary. The trivial solution does destabilize when the coupling is sufficiently strong. Profiles of solutions to this system are drawn in figure 4.2.1. For the lower ranges of c shown there is a stable stationary solution different from (4.25).

In the rightmost panel of figure 4.2.1 the solution converges to a continuous function. The solution also satisfies

$$0 = H(U(x)) + c \int_{\mathbb{R}} J(x-y) D(U(x) - U(y)) dy$$

however it is not of the type shown to exist by theorem 2. This solution is stationary because of symmetry about the values of x where $u(x,t)$ vanishes. This symmetry can be destroyed by shifting the interaction function, J, either left or right. Shifting left will result in a stronger influence of neighbors to the left. The result is a front the travels to the right. Similarly, shifting the function J right provides a mechanism for left-moving front solutions. Simulations of the network where J is shifted to the right are shown in figure 4.2.2.

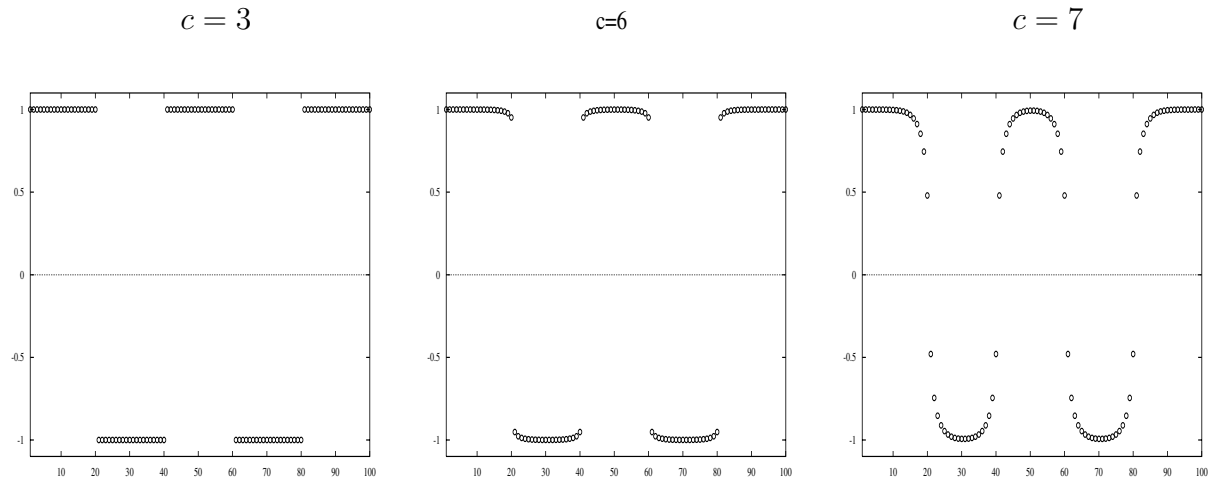

Figure 4.2.1: Profiles for steady state solutions for different coupling strengths. For small coupling coefficients the solutions lie near the fixed points of the uncoupled system. For larger coupling strengths the network will approach a more uniform profile. In the right panel the coupling is strong enough that the solution is continuous. The initial conditions for each of figures are slight perturbation from the known stationary solution $U(x)$.

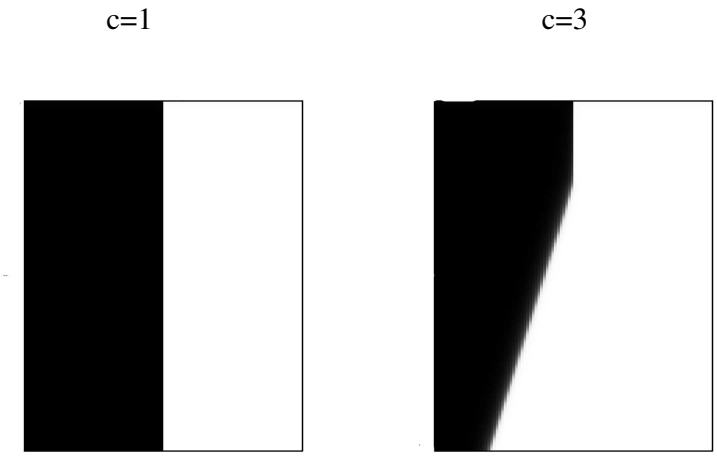

Figure 4.2.2: The waves resulting from biased coupling. In the left panel the stationary solutions continue to exist with bias coupling. In the right panel, the stationary solutions are destabilized. A left shift in J causes the network to bias to the left, causing a propagating wave. The long term solution is a uniform profile $u = -1$.

4.3 SUMMARY

In this chapter, we present a pair of models. The first is a network of integrate and fire nodes driven by a sinusoidal stimulus that is periodic in time and constant in space. The model is motivated by experiments performed by R.H.S. Carpenter. Our network is a rectangular grid of nodes with nearest neighbor coupling. In the absence of coupling each node is phase locked 1:2 with the driving stimulus. There are two such solutions, and the boundaries separating regions out of phase with one another represent the phosphenes reported by Carpenter's subjects. These lines are formed by passing a traveling inhibition through the network, causing half of the nodes to switch phases. The traveling inhibition is analogous to the retreating edge in the experiment. The coupling that we use encourages synchrony in the network. This causes a tug of war between the intrinsic dynamics of the system and the coupling architecture. Movement of the lines is modeled by coupling sufficiently strong to cause nodes near a phase boundary to leave the original basin of attraction and switch phases. Random bias in the coupling controls the movement of the boundaries.

The model demonstrates a mechanism suggested by Carpenter as a reason behind the creation of the phosphenes. The integrate and fire system was chosen for its simplicity, allowing us to determine parameter regimes that induce the desired phase locking. The coupling that we use is nearest neighbor. The type of coupling used could be expanded to include other configurations such as all to all coupling, where the strength of the interactions decays with distance. This model is an extreme simplification of the circuitry present in the retina. For example, the model does not take into consideration the different types of cells, such as H-cells and R-cells. We assume spatial independence of the driving stimulus, where

the action of the current on an individual cell may only involve a certain component, as described in [54]. Finally, the lines in Carpenter's experiment eventually fade away. This is impossible using our mechanism, since there is nothing in our model to associate with intensity.

The second model analyzed is an evolution/convolution network that captures the essential characteristics of the full model. The intrinsic bistability is represented by a pair of fixed points that are stable for the uncoupled system. As in the full model, the coupling encourages synchrony in the network. The interaction between the intrinsic dynamics of the network and the architecture of the coupling leads to various spatio-temporal patterns. We prove the existence and stability of discontinuous, time invariant solutions for sufficiently weak coupling. Numerically we suggest that biased coupling can cause waves to propagate when the coupling is sufficiently strong to eliminate the steady state solutions.

5.0 DISCUSSION

In this dissertation three coupled networks are analyzed. In each, the interplay between the intrinsic dynamics and the properties of the coupling result in various spatial patterns. In the first chapter of this work, we explore a system where the oscillations at each spatial location will decay to zero in the absence of coupling. The equation that we use is the normal form of a degenerate Hopf bifurcation, where the coefficient that determines the criticality of the resulting periodic solutions is zero. The coupling is of the correct order so that the degeneracy is removed. Under conditions on the parameters there are a pair of periodic solutions, as well as a rest state. It is shown that the outer periodic is linearly stable for sufficiently small wave numbers. This implies a region of bistability. We analyze solutions connecting the stable states. We show that, in the absence of twist, traveling waves exist and are stable. Numerical simulations suggest that with a nonzero phase gradient the waves continue to exist, provided the network along the wave front does not desynchronize too much. If the network does sufficiently desynchronize the effective coupling strength is too weak for the front to propagate. Locations that are already excited will remain on or near the outer periodic and the result is regions of persistent activity, or breathers.

There are a number of open problems in this chapter. The existence and stability of the breathers is not proved. We do unveil a lateral inhibition mechanism that, in other

scenarios, is known to generate localized activity. The inhibition is a result of a deviation from synchrony. For large phase gradients the effective interaction function can be approximated by a structure similar to a Mexican hat, where oscillations are excited by those nearby and inhibited by oscillations further away. A possible future direction is to determine, based on the parameters and initial conditions, the maximum width of a pulse. This would involve formulating a criterion for recruitment. When this criterion is not met the bump will propagate no further.

Similarly, there is no proof of existence for the waves when $q \neq 0$. We rely on continuity with respect to parameter changes, however the waves continue to exist for q well away from zero. A continuity argument is insufficient for such a case.

Lastly, a formal shooting argument could be made to verify the existence of traveling wave solutions for the $q = 0$ case when $\epsilon = 0$. The system of ODEs in traveling wave coordinates appears to have the desired heteroclinic, however we only suggest this numerically.

The second chapter is an exploration of a canard mechanism that contradicts widespread assumptions of excitatory synaptic coupling. In a typical scenario, excitatory coupling causes a network of type II neurons to synchronize. Once the network is synchronized it will either continue to spike or die, depending on whether the applied current is sufficient to pass threshold. In the case that the applied current is superthreshold, firing rate should increase. In a network of Hodgkin-Huxley neurons the oscillators synchronize, as expected. However, the amount of time that the oscillation spend in the silent phase is much longer than in the uncoupled network. The usual slow passage calculation does not provide an explanation for the long interspike intervals. A trapping mechanism that is the result of interplay between the intrinsic dynamics of a cell and the decay rate of a synaptic variable yields a curve that

acts as an attractor. Variational analysis along this curve provides a superior approximation of the local behavior and correspondingly a mechanism for the long ISIs.

The mechanism is unlike other canard scenarios because it is robust in the sense that it exists for a wide range of parameter values. An open problem would be to determine if a similar mechanism exists in the general canard configuration [15, 52]. Actual canard trajectories typically do not coincide with the critical manifold exactly except in the singular limit, where the system is decomposed into slow and fast subsystems. Revealing the general trapping mechanism that not only holds the solutions near the critical curve, but holds it away, would be a useful result.

The third problem presented is a network that is intrinsically bistable, and the coupling causes the network to synchronize. There are two models presented. The first is a network of integrate and fire oscillators where the attractors are a pair of solutions phase locked with a driving stimulus. We compare the patterns that solutions to this network form to those reported by subjects in an experiment preformed by R.H.S. Carpenter. The second model is an evolution/convolution equation that captures the basic properties of the full equations: it is intrinsically bistable with coupling that causes synchrony. The resulting tug of war results in stable steady state solutions when the coupling is sufficiently weak and, for stronger coupling, traveling waves connecting the stable states. We present proof for the existence and stability of the steady state solutions.

The model that we present to model the experiment of Carpenter is sufficient to recreate the pattern reported by subjects. However, the model is an extremely crude representation of the physiology of the retina. A more elaborate model that more closely represents the communication in the retina and demonstrates the same results would be an extremely useful

result.

An open problem regarding the reduced model is the existence and stability of traveling wave solutions when the interaction independent stationary solutions no longer exist.

APPENDIX

PARAMETERS AND GATING FUNCTIONS FOR THE HH EQUATIONS

The gating functions for h in equation (3.3) are

$$\alpha_h(V) = 0.07 \exp\left(-(V+65)/20\right)$$

$$\beta_h(V) = 1/\left(1 + \exp(-(V+35)/10)\right)$$

The variable m is slaved to V

$$m = \frac{\alpha_m(V)}{\alpha_m(V) + \beta_m(V)}$$

where

$$\alpha_m(V) = \frac{0.1(V+40)}{1 - \exp(-(V+40)/10)}$$

$$\beta_m(V) = 4 \exp(-(V+65)/18)$$

The variable n is slaved to h by

$$n = \max(.801 - 1.03h, 0)$$

The synaptic recovery function, $\alpha(V)$, is given by

$$\alpha(V) = \frac{\alpha_0}{1 + \exp(-V/V_{shp})}$$

Parameter values are $V_{Na} = 50$, $V_k = -77$, $V_L = -54.4$, $g_{Na} = 120$, $g_K = 36$,$g_L = 0.3$,$C = 1$,$I_0 = 13$, $V_{shp} = 5$, $g_{syn} = 2$, $V_{syn} = 0$, and $\alpha_0 = 2$.

The units for the voltages are mV, the conductances have units mS/cm^2, and the current has units $\mu A/cm^2$.

BIBLIOGRAPHY

[1] Shun-ichi Amari, *Dynamics of Pattern Formation in Lateral-Inhibition Type Neural Fields*, Bio Cybernetics (1977)

[2] D.G. Aronson, G.B. Ermentrout, and N Kopell, *Amplitude response of Coupled Oscillators*, Phs. D, 41 (1990), pp. 403-449

[3] Kendall E. Atkinson, *An Introduction to Numerical Analysis,* John Wiley & Sons, Inc. 1989

[4] S.M. Baer, T. Erneux, and J. Rinzel, *The slow passage through a Hopf bifurcation: Delay, memory effects and resonance*, SIAM J Appl Math. 49 (1989), pp.55-71

[5] Bates, Peter W and Chmaj, Adam *An Integrodifferential Model for Phase Transitions: Stationary Solutions in Higher Space Dimensions* Journal of Statistical Physics 95, 1119-1139 (1999)

[6] P.W. Bates and A. Chmaj, *A discrete convolution model for phase transitions*, Arch. Rational Mech Anal. 150 (1999) pp. 281-305

[7] G.S. Brindley, *The site of electrical excitation of the human eye*, J. physiol. 127 (1955), pp. 189-200

[8] M. Camperi and X.J. Wang, *A model of visuospatial short-term memory in prefrontal cortex: Cellular bistability and recurrent network*, J. Comput. Neurosci, 5 (1998), pp. 383-405

[9] Carpenter, R.H.S. *Contour-Like Phosphenes From Electrical Stimulation of the Human Eye: Some New Observations*, J. Physiol. 229, 767-785 (1973)

[10] X. Chen, *Existence, Uniqueness, and Asymptotic Stability of Traveling Waves in Nonlocal Evolution Equations*, Adv. Differential Equations 2 (1997), pp. 125-160

[11] X. Chen and G.B. Ermentrout, *Wave propagation mediated by $GABA_B$ synapse and rebound excitation in an inhibitory network: A reduced model approach*, J. Comput Neurosci., 5 (1998) pp. 53-69

[12] A. Compte, N. Brunel, P.S. Goldman-Rakic, X.J. Wang, *Synaptic mechanisms and network dynamics underlying spatial working memory in a cortical network model*, Cerebral Cortex, 10 (2000), pp. 910-923

[13] Crevier, Daniel W. and Meister, Markus *Synchronous Period-Doubling in Flicker Vision of Salamander and Man*

[14] Diener, F., Diener, M., *Maximal Delay*, in Dynamic Bifurcations, E. Benoit, ed., Lecture Notes in Math. 1493, Springer, NY, 1993, pp. 71-86.

[15] Diener, M. *The Canard Unchained or how Fast/Slow Dynamical Systems Bifurcate*, Math. Intell., 6 (1984), pp. 38-49

[16] E. Doedal, *AUTO: A program for the automatic bifurcation analysis of autonomous systems*, Congr. Numer., 30 (1981), pp. 265-284

[17] Drover, J., Rubin, J., Su, J., and Ermentrout, B, *Analysis of a Canard Mechanism by which Excitatory Synaptic Coupling can Synchronize Neurons at Low Firing Frequencies*, SIAP 65, No. 1 pp. 69-92

[18] Drover, J. Ermentrout, B., *Nonlinear Coupling near a Degenerate Hopf (Bautin) Bifurcation*, SIAP 63, No. 5, pp. 1627-1647

[19] Doi, S., Kumagai, *Nonlinear Dynamics of Small Scale Biophysical Neural Networks*, Biophysical Neural Networks, Mary Ann Liebart Inc., Larchmont, NY, 2001, pp. 261-297

[20] Ermentrout, G.B *n:m Phase-Locking of Weakly Coupled Oscillators* J. Math. Biology 12, 327-342 (1981)

[21] Ermentrout, B, *Simulating, Analyzing, and Animating Dynamical Systems: A Guide to XPPAUT for Researchers and Students*, Software Environ Tools 14, SIAM, Philadelphia, 2002

[22] G.B. Ermentrout, *Stable small amplitude solutions in reaction diffusion systems*, Quart Appl Math, 39 (1981), pp.61-86

[23] G.B. Ermentrout, X. Chen and Z. Chen, *Transition fronts and localized structures in bistable reaction-diffusion equations*, Phys D, 108 (1997), pp. 147-167

[24] Ermentrout B. and Lewis M. *Pattern formation in systems with one spatially distributed species*. Bulletin of Mathematical Biology 59: 533-549 (1997)

[25] B. Ermentrout, *Type I membranes, phase resetting curves, and synchrony*, Neural Comput. 8 (1996), pp. 979-1001

[26] Golomb, D. and Amitai, Y. Propagating neuronal discharges in neocortical slices: Computational and experimental study. *J. Neurophysiol.* 78:1199-211 (1997)

[27] Yixin Guo, *Existence and stability of standing pulses in neural networks* PhD. Dissertation, University of Pittsburgh electronic thesis

[28] B.S. Gutkin, C.R. Laing, C.L. Colby, CC. Chow, G.B. Ermentrout, *Turning on and off with excitation: The role of spike timing asynchrony and synchrony in sustained neural activity*, J Comput Neurosci, 11 (2001), pp. 121-134

[29] D. Hansel, G. Mato and C. Meunier, *Phase Dynamics for Weakly Coupled Hodgkin-Huxley Neurons*, Europhys. Letters 23 (1993) p. 367

[30] D. Hansel, G. Mato, and C. Meunier, *Synchrony in excitatory neural networks*, Neural Comput, 7 (1995), pp. 307-337

[31] D. Hansel and G. Mato, *Existence and Stability of Persistent States in large neuronal networks*, Phys rev Lett, 86 (2001) pp. 4175-4178

[32] A.L. Hodgkin and A.F. Huxley, *A quantitative description of the membrane current and its application to conduction and excitation in nerves*, J. Physiol (Lond.), 117 (1952), pp. 500-544

[33] F.C. Hoppensteadt and E.M. Izhikevich, *Weakly Connected Neural Networks*, Springer Verlag, New York, 1997

[34] Po-Fang Hsieh and Yasutaka Sibuya, *Basic Theory of Ordinary Differential Equations*, Springer Verlag, New York, 1999

[35] Izhikevich E.M. *Class 1 Neural Excitability, Conventional Synapses, Weakly Connected Networks, and Mathematical Foundations of Pulse-Coupled Models* . IEEE Transactions On Neural Networks,10:499-507 (1999)

[36] Izhikevich E.M. *Neural Excitability, Spiking, and Bursting*. International Journal of Bifurcation and Chaos. 10:1171-1266 (2000).

[37] Izhikevich E.M. *Subcritical Elliptic Bursting of Bautin Type*. SIAM Journal on Applied Mathematics, 60:503-535 (2000)

[38] Yuri Kuznetsov, *Elements of Applied Bifurcation Theory*, Springer-Verlag, New York, 1998

[39] Laing, C. and Chow, CC, *Stationary bumps in networks of spiking neurons*. Neural Computation 13:1473-94 (2001)

[40] Loewenstein Y, Sompolinsky H. Oscillations by symmetry breaking in homogeneous networks with electrical coupling. Phys Rev E 65:51926 (2002)

[41] Neishtadt, A.I., *Prolongation of the Loss of Stability in the Case of Dynamic Bifurcations. I.*, Differential Equations, 23 (1987), pp. 1385-1390.

[42] Neishtadt, A.I., *Prolongation of the Loss of Stability in the Case of Dynamic Bifurcations. II.*, Differential Equations, 24 (1988), pp. 171-176

[43] Pinto, D. Ermentrout, G.B. *Spatially Structured activity in synaptically coupled neural networks: I. Traveling fronts and pulses*, SIAM J. Appl Math, 62 (2001) pp. 206-225

[44] Rinzel, J and Ermentrout, B, Analysis of Neural Excitability and Oscillations, in *Methods in Neuronal Modeling: From Ions to Networks*, (Christof Koch and Idan Segev, eds), Chapter 7, MIT Press, Cambridge, MA (1998)

[45] J. Rinzel, *Excitation dynamics: Insights from simplified membrane models*, Fed. Proc. 44 (1985), pp. 2944-2946

[46] Rubin, J., *Surprising effects of Synaptic Excitation*, J. Comp. Neurosci. 18 (2005) pp. 333-342

[47] Rubin, J., Bose, A., *Localized Activity Patterns in Excitatory Neuronal Networks*, Network: Comput Neural Syst 15 (2004) pp. 133-158

[48] D. Somers and N. Kopell, *Rapid synchronization through fast threshold modulation*, Biol Cybern, 68 (1993), pp. 393-407

[49] R.D. Traub and R. Miles *Neuronal Networks of the Hippocampus*, Cambridge University Press, UK, 1991

[50] Wang X.-J. Synaptic basis of cortical persistent activity: the importance of NMDA receptors to working memory. J. Neurosci. 19, 9587-9603 (1999)

[51] David I Schwartz, *Introduction to Maple 8,* Pearson Education, Ind, NJ. 2003

[52] Szmolyan, P, Wechselberger, M., *Canards in* $\mathbb{R}^3$, J. Differential Equations, 177 (2001) pp. 419-453

[53] S. Wiggins, *Introduction to Applied Nonlinear Dynamical Systems and Chaos*, Springer-Verlag, New York, 1990

[54] Willis, J.B. *The Modeling of Neural Circuitry* Progress in Neurobiology, 26, 93-118 (1986)